Ultrasonic Testing in Battery Research and Production

Sam Amsterdam,[1+] Aamani Ponnekanti,[2+] Nicolina Nanni,[3] Andrew Hsieh,[3] Robin James,[4] Erik Huemiller,[4] Daniel A Steingart,[2] Wesley Chang[1]*

1. Department of Mechanical Engineering and Mechanics, Drexel University, Philadelphia, Pennsylvania, United States

2. Department of Chemical Engineering, Columbia University, New York, New York, United States

3. Liminal Insights, Inc, Emeryville, California, United States

4. General Motors Research & Development, Warren, Michigan, United States

+ These authors contributed equally to this work

*Corresponding author

Context and Scale

The increased adoption of lithium-based rechargeable batteries requires advanced metrology tools across the entire battery lifecycle. Ultrasound testing (UT) has emerged as a promising, low-cost, and scalable technique for providing valuable insights at various stages of battery development and operation. This review highlights the fundamental principles of UT and its diverse applications, spanning from lab-scale research to manufacturing and field-deployed monitoring. In addition to a synthesis of the existing battery UT literature, including acoustic detection of battery failure modes and decoupling different physical phenomena, we emphasize emerging battery UT methods and applications. For instance, recent advances in ultrasonic transducer technology may be adapted for enhancing battery UT resolution. UT techniques could be used not only for battery cell characterization but also for in-line monitoring of slurry quality and electrodes. Lastly, we draw connections from lab-scale research and development to in-line quality assurance and metrology on the industrial scale. Underscoring this is a discussion of current challenges, including signal processing complexity, the need for large datasets, and, especially pertinent to manufacturing and field-deployed applications, cost and throughput. Addressing these issues through methods such as new signal processing techniques, machine learning, and advanced sensors will help drive UT's adoption for batteries at industrial scale.

Abstract

This review provides a comprehensive overview of ultrasonic testing (UT) applied to battery research and development, bridging the gap between fundamental acoustic principles and practical applications. We begin by detailing the acoustic physics underlying UT and describing the hardware, software, and signal processing algorithms necessary to extract useful information from battery systems. We then summarize key academic findings and trends in UT analysis of lithium-based batteries, highlighting both foundational studies that have shaped the field and recent advancements pushing the boundaries of UT application. Following this, we provide an overview of lab-scale *operando* tools that complement UT analysis, illustrating how they can enhance and validate its findings. The discussion is extended beyond academic work to encompass UT applications in battery manufacturing, uniquely incorporating industry perspectives on the challenges and opportunities in this space. Finally, we conclude with a discussion of future directions in battery UT research. This review aims to provide a summary of the current state of UT applied to

batteries, equip readers with the tools to contextualize new UT studies and applications, and serve as a practical guide for researchers and engineers seeking to implement UT in their work.

Graphical Abstract

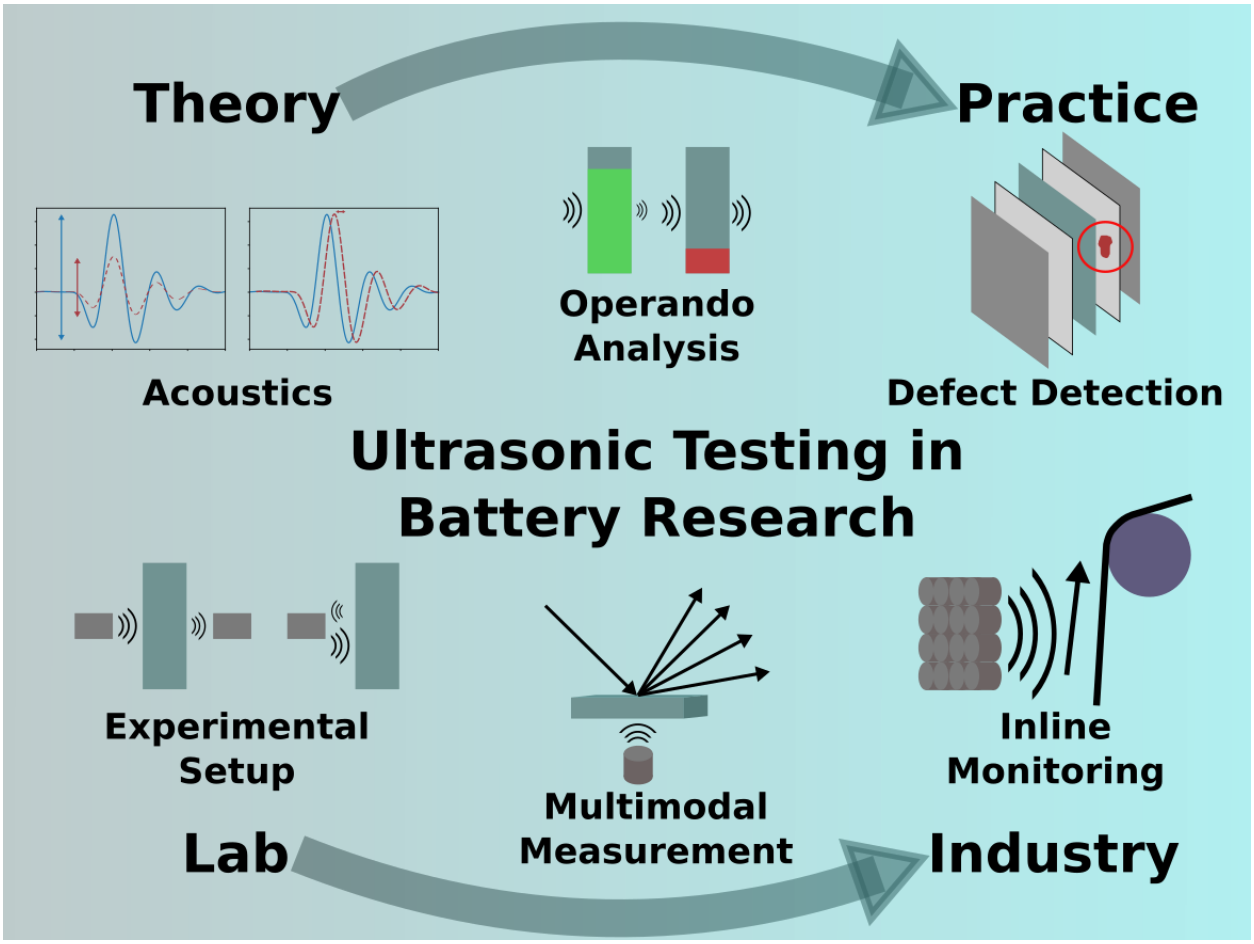

Glossary

UT: Ultrasonic testing
BMS: Battery management system
NDE: nondestructive evaluation
SNR: signal-to-noise ratio
LCO: lithium cobalt oxide
TOFD: time-of-flight diffraction
SAM: scanning acoustic microscopy
EMAT: electromagnetic acoustic transducers
CMUT: capacitive micromachined ultrasonic transducers
PRF: pulse repetition frequency
SA: signal amplitude

ToF: time-of-flight
SoC: state of charge
SoH: state of health
NMC: nickel manganese cobalt oxide
LFP: lithium iron phosphate
LTO: lithium titanate oxide
SEI: solid-electrolyte interphase
OCV: open circuit voltage
TR: thermal runaway
AE: acoustic emission

Introduction

The escalating demand for batteries, projected to reach at least 2500 GWh by 2030,[1] necessitates rapid innovation across all stages of battery technology. Research into novel materials, as well as how and why current systems fail, is crucial. At the same time, industry requires improvements in manufacturing processes like slurry control and formation monitoring. With the increasing numbers of field-deployed batteries for diverse applications, battery management systems (BMSs) that ensure safe operation are also vital. A common thread linking these efforts is the urgent requirement for high-performance, cost-effective, high-throughput characterization tools to accelerate innovation and meet the ever-increasing demand.

Ultrasonic testing (UT) is a mature nondestructive evaluation (NDE) technique used in diverse fields from medicine to construction, and it has recently been adopted for a wide range of battery applications. UT is an active method that interrogates systems using acoustic waves at frequencies above 20 kHz.[2] The resulting waveforms contain valuable information about internal conditions, material properties, and the evolution of defects. The external nature of the transducers and low energy of the ultrasonic pulses enable nondestructive and *operando* measurements at a relatively low cost compared to other characterization techniques. Although the mechanical insights of UT alone are valuable, using this technique in conjunction with other measurements can provide a rich picture of battery dynamics. In addition to assembled batteries, manufacturing lines can integrate UT for rapid, in-line quality control at various stages of production.

This review highlights fundamental principles, implementation strategies, and applications of UT in battery manufacturing and production processes. This review is organized into the following sections: ultrasound theory, UT hardware and signal processing, overview of prior studies on batteries, integration of UT with other *operando* techniques, and battery industry applications of UT. We conclude this review by discussing future applications and perspectives. We intend to complement previous reviews by Majasan et al.,[3] McGovern et al.,[4] and Deng et al.[5] by highlighting recent advancements. We also go beyond research to incorporate discussions of manufacturing and field-deployed applications, combining perspectives from academia and industry on the current state of the art, near-future research directions, and bottlenecks to widespread application. This review is intended as a guide for battery scientists seeking to understand the capabilities of UT as well as researchers aiming to implement UT in their own work.

Ultrasound Theory Applied to Batteries

This section provides the basics of ultrasonic propagation and how it extends to complex systems like battery cells. UT operates on the basic principle that material properties in the acoustic path affect the propagation behavior of sound waves. Sound waves are simply pressure waves, so their behavior is directly related to the ability of vibrational energy to travel through the medium(s) in the acoustic path.

Longitudinal waves are most commonly analyzed for UT, though shear and surface waves are sometimes used. As shear waves attenuate rapidly in fluids, they are less applicable to battery cell systems as they cannot propagate through materials such as couplant, electrolytes, and gas pockets. Surface waves are less often discussed for battery applications, but are briefly mentioned in future sections due to their applications in guided wave analysis.[2] Here, we focus our discussion on longitudinal waves due to their prevalence in battery applications.

The speed of sound (c, m/s) is dictated by the material properties of the medium and the nature of the vibration, or type of sound wave. For longitudinal waves, this relationship is captured by the Newton-Laplace equation (Eqn. 1):

$$c = \sqrt{\frac{E(1-\nu)}{\rho(1-\nu-2\nu^2)}} \quad (1)$$

Here E is the Young's modulus, ν is Poisson's ratio, and ρ the density.[6] Increasing Young's modulus (stiffer material) or decreasing density results in a faster speed of sound. This equation assumes negligible local density changes, valid for frequencies > 1 MHz, typically used for UT on battery systems.[7] The reader is referred to Kinsler et al.[8] for a derivation of these relationships from the fundamental wave equations.

As a waveform propagates through the system, it experiences attenuation, in which energy is lost to the system. The sensors used in UT typically measure amplitude, which represents the sound wave pressure. Signal intensity, or energy, is proportional to the square of acoustic pressure.[2] As energy is lost, the measured signal amplitude (SA) decays exponentially with respect to the distance traveled, as described by the following equation (Eqn. 2):

$$A = A_0 e^{-\alpha z} \quad (2)$$

Where A_0 and A are the initial and final amplitudes, respectively, α is the attenuation coefficient, and z is the distance traveled.[2] Attenuation can result from scattering in media containing heterogeneities such as grain boundaries, defects, and porosity, or due to absorption, where elastic properties dissipate ultrasound energy as heat.[4]

As acoustic waves interact with interfaces within the system at normal incidence, the energy of the waves is partitioned based on the acoustic impedance difference between the subsequent materials. For a waveform with normal incidence to the interface between materials 1 and 2, the ratios between incident acoustic pressure (P_0) to transmitted pressure (P_T) (Eqn. 3) and reflected pressure (P_R) (Eqn. 4) are defined as follows:[4,5]

$$\frac{P_T}{P_0} = \frac{2Z_2}{Z_2+Z_1} \quad (3)$$

$$\frac{P_R}{P_0} = \frac{Z_2-Z_1}{Z_2+Z_1} \quad (4)$$

$$Z_i = \rho_i c_i \quad (5)$$

Here, Z_i is the material acoustic impedance, which is a function of ρ_i (density) and c_i (speed of sound) of the material i (Eqn. 5). These equations indicate that a greater mismatch between the acoustic impedance of subsequent layers results in greater reflection and less transmitted signal. Ultrasound waves can also experience refraction and mode conversion into different wave types at interfaces. For a complete derivation of these equations, we refer the reader to Ensminger et al.[2]

The ultrasound wavelength (λ) relative to the characteristic feature size of the system under study is of fundamental importance. This is related to frequency (f) and speed of sound (c) (Eqn. 6):

$$\lambda = \frac{c}{f} \quad (6)$$

As with other wave phenomena, higher frequencies yield smaller wavelengths. Similar to optics, smaller wavelengths can resolve finer feature resolution in the acoustic signal, as dictated by the following equation (Eqn. 7):[9,10]

$$W = \frac{\lambda}{2 \times N.A.} \sim \frac{\lambda}{2} \quad (7)$$

Here, W is the minimal detectable feature size, and N.A. is the numerical aperture of the transducer, which is hardware-dependent, though resolution is typically estimated to be half of the wavelength. On the other hand, higher frequencies can increase scattering and absorption contributions, attenuating the signal and decreasing signal-to-noise ratio (SNR). As such, optimization of f and consequently λ is crucial for UT analysis.

The heterogeneous nature of batteries increases the complexity of UT analysis. A typical battery comprises a repetitive, finely layered structure, which results in different waveform propagation than a bulk, homogenous material would demonstrate. Furthermore, battery electrodes and separator materials are porous solids filled with fluid, which behave differently than homogenous solids. Finally, the electrodes themselves are composite materials made up of active material, conductive additives, and binders. In reality, Eqn. 1 needs to be adjusted to account for the effect of porosity, the different values of Young's modulus and density for each material, and the effect of layers on waveform propagation. Practically speaking, experimental UT papers simplify this by discussing the effective elastic modulus, or effective stiffness (E_{eff}) of the system, and the overall system density (ρ):[6,11]

$$c = \sqrt{\frac{E_{eff}}{\rho}} \quad (8)$$

Throughout this review, we will use E to refer to the Young's modulus of a pure material and E_{eff} to refer to the effective stiffness of an electrode film. This assumes that the system is an isotropic, homogeneous solid.[6,7] This is generally accepted if the ratio of the wavelength to the individual layer thicknesses is sufficiently large (5-8).[6] **Table 1** shows the wavelengths for medium- and high-frequency waves passing through common battery components. We show both individual materials and composite electrodes, as well as a full cell with electrolyte. While material properties vary across studies with factors including measurement method, manufacturer, and composition, these values provide a rough comparison between frequency-dependent wavelength and layer thickness.

Table 1. Material properties, sound speed (c), and frequency-dependent wavelengths of lithium cobalt oxide (LCO) || graphite cell components at 0 % state-of-charge. For single materials, c is calculated from Young's modulus (E) and Poisson's ratio (ν). For composite electrodes, the measured effective moduli (E_{eff}) incorporate the current collector, binder, conductive additives, and electrolyte. For the full cell, E_{eff} also includes the separator. Wavelengths are compared with typical layer thicknesses reported in the literature.

Material	**E (GPa)**	ν	ρ **(g/cm^3)**	**c (m/s)[a]**	**λ (µm) @ 2.25 MHz[b]**	**λ (µm) @ 15 MHz[b]**	**Layer Thickness (μm)**

Graphite	32[12]	0.32[12]	2.26[13]	4500	2001	300	65.5[14]-96[15]
LCO	178±5 [16]	0.3[16]	4.46[17]	6990	3110	466	46.5[14]-60[15]
Copper	124±0.7 [18]	0.350± 0.009[18]	8.93[19]	4710	2090	314	8[14]-10[15]
Aluminum	69[19]	0.33[19]	2.71[19]	6140	2730	409	10[15]-12[14]
Celgard	0.55[14]	0.35[14]	0.75[14]	1084	482	72.3	15[14]-25[15]
	E_{eff} (GPa)		**ρ (g/cm^3)**	**c (m/s)[c]**	**λ @ 2.25 MHz[b]**	**λ @ 15 MHz[b]**	**Layer Thickness (μm)**
Composite Graphite/Cu	10.7[7]		1.06[7]	3180	1410	211	200[7]
Composite LCO/Al	27.8[7]		1.54[7]	4250	1890	283	180[7]
LCO || Graphite Cell	4.76[7]		1.60[7]	1720[7]	767	114	170[7]

[a]calculated from Eqn 1.
[b]calculated from Eqn 6.
[c]calculated from Eqn 8.

Based on the wavelengths and typical layer thicknesses presented in **Table 1**, this assumption of the battery as a homogenous solid holds at medium frequencies (2.25 MHz) but loses accuracy at higher frequencies (15 MHz). The implication of this from a practical standpoint is that higher frequencies can generate greater scattering contributions and produce acoustic responses that are less representative of average cell properties, although they may better resolve microstructure and small features. In addition to the tradeoff between resolution and attenuation, this factor must be considered when choosing UT frequency.

Generating and Measuring Ultrasound

The instrumentation used to conduct an ultrasound experiment is relatively straightforward. The fundamental components are a pulse generator, transducer(s), and a recording device. Several vendors exist for pre-built UT instruments, but simple lab-built systems can also produce high-quality data at a far lower

cost.[20,21] This section will discuss the physical layout of various UT setups and review some experimental choices related to hardware selection. Special attention is paid to transducer selection, with an eye towards future applications of advanced transducer technology to battery research.

Ultrasound Testing Modes

Ultrasonic measurements rely on a transducer that converts electrical signals into acoustic waves and vice versa. The type and placement of these transducers are carefully chosen to optimize signal collection for the system and features of interest (**Figure 1a**). Two primary measurement modes are used for UT in battery systems: through-transmission and pulse-echo. Through-transmission, or simply transmission, utilizes a separate transmitting and receiving transducer. The transducers are placed across from each other such that the received signal is a combination of the signal entirely transmitted through the battery and internal and surface reflections. Though individual signal features are difficult to correlate to specific internal structures, transmission can provide information on the average material properties of the entire through-thickness of the cell in the direction of acoustic propagation.[22] On the other hand, the necessity of this signal to pass through the entire system requires lower frequencies to reduce attenuation, which limits feature resolution. 2.25 MHz has been found empirically to provide a good tradeoff between resolution and SNR for most pouch cells, though other frequencies are often used.[23,24] Frequency-dependent transmission measurements can also be performed to identify acoustic resonances within the cell.[23,24] The transducers are typically aligned in a transmission measurement, though useful information about scattering can also be gathered by using a receiving transducer that is axially offset from the sending transducer.

In contrast, pulse-echo, or reflection, involves one transducer that transmits and receives the reflected acoustic signal. Pulse-echo datasets contain a series of reflections from various interfaces within the cell. Decoupling these reflections can allow for specific regions or features to be isolated. At deterministically low frequencies, the signal can penetrate the whole cell and reflect to the transducer, often called the back-wall reflection or first echo.[25] Analyzing the first echo yields information similar to through-transmission since it has interacted with the entire cell. Pulse-echo can also utilize higher frequencies, sometimes up to 25 MHz,[26] to achieve greater resolution of small-scale defects and phenomena, though the resulting attenuation can limit the penetration depth.[22,27] While pulse-echo datasets may contain more information than through-transmission due to the ability to decouple different reflections, the increased number of reflections can yield lower SNR and more difficult signal deconvolution. Thus, the choice of pulse-echo and through-transmission depends on the system and desired analysis. Fortunately, with the right hardware, it is straightforward in most cells to operate both simultaneously.

The previously mentioned modes rely on normal incidence waves, in which the signal is sent and received at a 90-degree angle to the battery surface. Additionally, there is a diverse body of literature on oblique waves. In pitch–catch configurations, one transducer transmits while one or more receivers collect signals at different angles. Using multiple receivers on the same or opposite sides of a battery enables analysis of multiple propagation paths and larger interrogation areas. A typical application of pitch-catch is guided wave analysis.[15,28] This method has been cited to utilize less bulky acoustic probes and capture greater areas with less attenuation. This can be valuable for field-deployed systems. However, guided waves support multiple modes, including diffracted and surface waves, which complicates interpretation, and typically operate at lower frequencies (~60–200 kHz), thereby reducing spatial resolution.[15] To date, battery studies have focused on planar geometries (pouch and prismatic cells), where guided waves propagate most effectively, although cylindrical configurations have been explored in structural NDE.[29] Another application of pitch-catch is time-of-flight diffraction (TOFD), which uses contact transducers on the same side to determine the size of an internal crack by comparing the arrival time of waves diffracted from the top and bottom of the crack.[30] This is often used for the evaluation of weld quality.

While informative studies are done on a single point of a battery, it is also common to collect spatially resolved information (**Figure 1b**). In scanning acoustic microscopy (SAM), this is typically done by attaching the transducers to a gantry and rastering across the cell. Data is often collected in through-transmission or pulse-echo mode, achieving millimeter-to-micron resolution depending on transducer, coupling medium, and signal processing. This will be discussed further in the next section. Collection times are limited by gantry scan speed and measurement time at each individual point. This can introduce temporal heterogeneities within a scan, particularly for fine spatial resolution or large scan areas. This is a hindrance for in-line applications, making SAM collection speed a major area of research.

Many transducers can be used simultaneously as an array to increase the acquisition speed. These can be operated as multiple elements all conducting transmission or pulse-echo.[31] and they can be rastered to increase SAM acquisition speed. Often in the battery literature, they are operated as phased arrays (**Figure 1c**). These work by adjusting the time delay between neighboring transducers such that the resulting interference pattern produces a single acoustic wavefront across the width of the array.[32] Manipulating the delays can change the angle of the ultrasonic pulse with respect to the transducer, allowing large areas to be scanned without needing to move the transducers physically.[32] Beam steering and dynamic focusing also enables resolution of depth-dependent features.[33] There is growing interest in applying these arrays for battery research due to their higher speed operation, which is useful for large battery formats and rapid in-line characterization, and they have been successfully used to monitor defect formation,[34] gas generation,[33,35], and state of charge (SoC).[36] Thin micromachined arrays also offer more compact, field-deployable options, though typically at lower frequencies.[31] Still, the increased data complexity and higher cost of arrays can limit applications. The tradeoffs of single-point and spatially-resolved methods are summarized in **Table 2**.

Table 2. Summary of advantages and disadvantages of single-point, SAM, and array systems.

Method	**Advantages**	**Disadvantages**
Single-point	Minimal and low-cost equipment requirements; small hardware footprint enables integration with many systems	Lack of spatial resolution limits analysis of heterogeneous or localized phenomena
SAM	Provides spatial resolution; commercial systems available; can be built in-lab at lower cost than most spatially resolved *operando* characterization methods	Tradeoffs between spatial and temporal resolution governed by scan speed and area; scanning may be infeasible in some systems; coupling while scanning requires non-contact immersion or air-coupled transducers, or using more complex dry coupled rollers; increased data volume
Array	Enables rapid spatial analysis without temporal variation; phased arrays can resolve depth-dependent features; stationary probes facilitate integration with many systems	Tradeoffs between hardware footprint and frequency; higher cost; increased data volume and analysis complexity

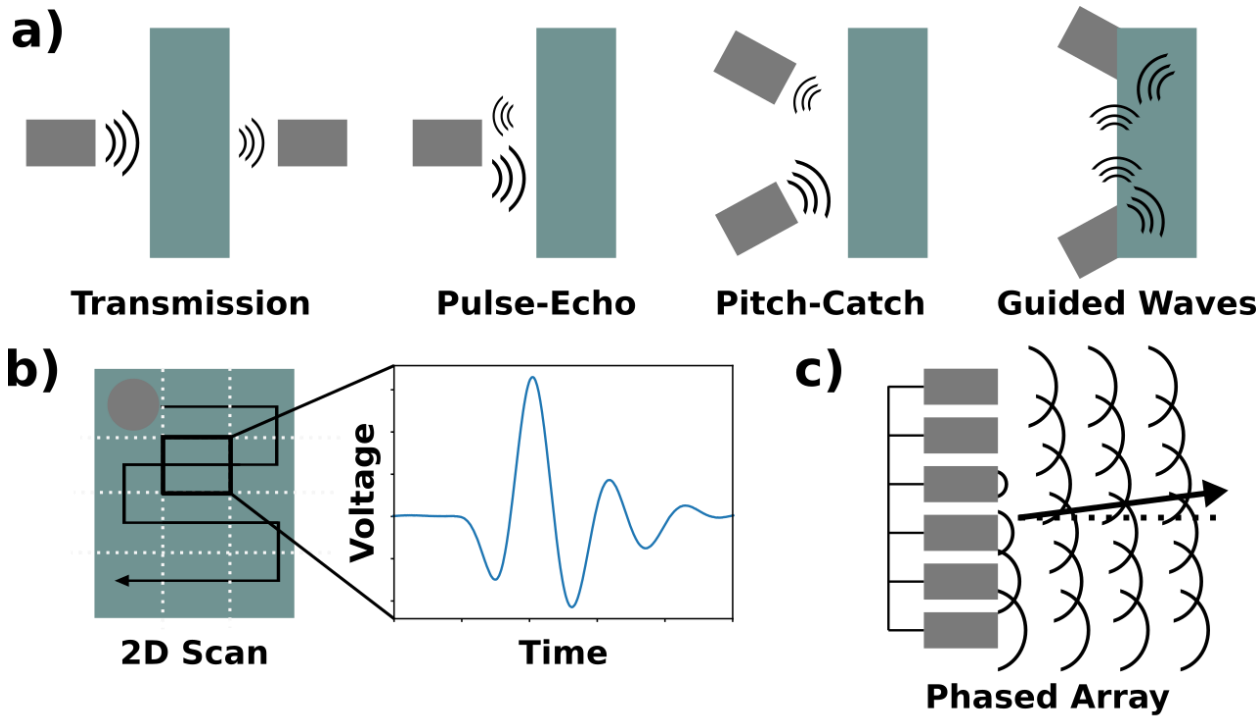

Figure 1. a) Schematic of the different UT collection modes. b) Schematics of 2D scanning or rastering with a single transducer to perform SAM. This produces an image where each pixel contains a full ultrasonic data waveform. c) Simplified schematic of the operation of a phased array transducer.

Types of Transducers

Transducers can be categorized by the physical mechanism of transduction, which affects the ultrasonic frequency, efficiency of generation and detection, and the requirements for coupling to the sample. The most relevant transducer types discussed in this review are shown in **Figure 2a**: piezoelectric crystals, electromagnetic acoustic transducers (EMAT), laser ultrasound, and capacitive micromachined ultrasonic transducers (CMUT).

The most common ultrasonic transducer is the piezoelectric crystal. A helpful introduction to piezoelectric transducers can be found in Shung and Zipparo,[32] but we will summarize a few relevant points here. The physical mechanism of these transducers is the piezoelectric effect, which occurs in materials with aligned internal dipole moments. The aligned dipole moments allow them to interconvert between pressure and electrical potential since any voltage exerts a force on the dipoles, and any change in the dipole moment generates a voltage. The most commonly used piezoelectric materials for ultrasound are lead zirconium titanate (PZT) ceramics and polyvinylidene difluoride (PVDF) based polymers. A piezoelectric crystal will have a resonant frequency that depends on its geometry, which results in ultrasonic transducers having limited bandwidth around a central frequency. Piezoelectric transducers typically produce longitudinal waves, though specialized shear transducers are available.

Coupling of the transducer to the sample is another design consideration. Choice of couplant is important to reduce signal loss due to reflection at the transducer surface and attenuation due to air gaps at the sample-transducer interface (**Figure 2b**). The couplant can be a gel for direct contact, a pad for solid coupling, a fluid like water or mineral oil for immersion transducers, or air for air-coupled transducers. Dry coupling strategies have also been commercialized using a transducer immersed in silicone oil encased in rubber

which is pressed onto the battery.[37] The rubber case can be used as a roller, enabling transducer scanning without the disadvantages of fluid or air coupling. In all cases, the acoustic impedance of the transducer face should be matched to the sample or couplant to maximize transmission. Since the acoustic impedance of a given piezoelectric material is a fixed property, matching layers are often added to the transducer to move the impedance closer to the target material. This means that a transducer designed for water immersion, for example, will not be interchangeable with one intended for use in air or for direct contact with metal.

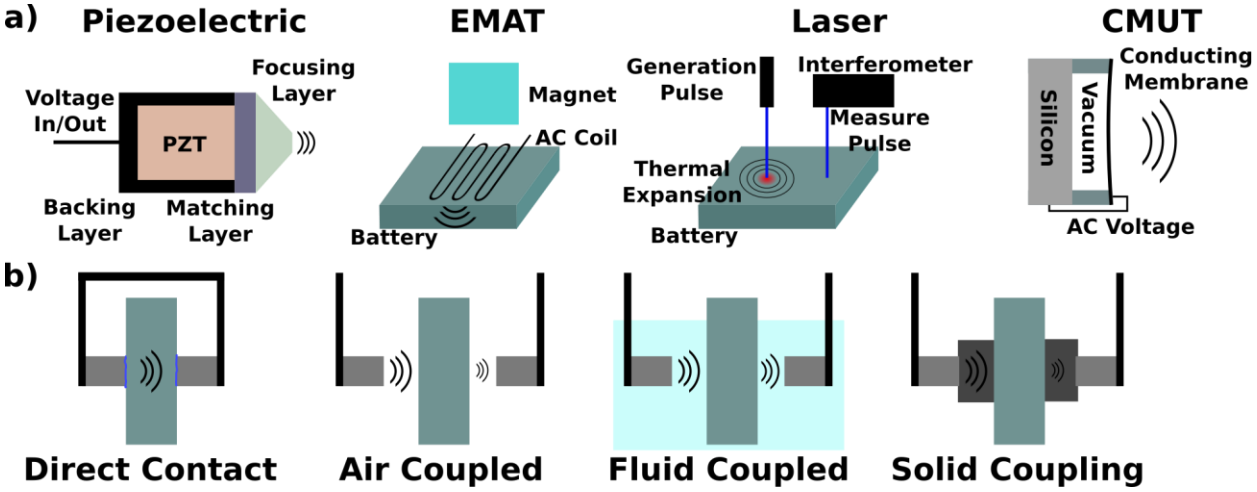

Figure 2. a) Categories of ultrasonic transducers and their operating principles. b) Types of sample – transducer coupling for piezoelectric and CMUT transducers. Note that both direct contact and solid coupling require the transducer to be pressed into the sample. In direct contact, a small amount of a coupling gel is sometimes used, while solid coupling uses a secondary material such as a rubber mat between the transducer and the sample.

In addition to improving coupling, material layers can be added to the transducer to shape the ultrasonic beam. These can be understood analogously to optical lenses, and enable cylindrical beams with minimal divergence, or beams that are focused to a line or point for improved spatial resolution. Analogous to optical microscopy, focused transducers can be used in SAM to produce near diffraction-limited images with spatial resolution on the order of wavelength divided by two (Eqn. 7), i.e. tens to hundreds of microns, depending on the frequency and propagation medium. Transducers designed for contact pulse-echo applications may also have a delay line attached, which adds material for the ultrasound to pass through before contacting the sample. This adds a delay between the generating pulse and the measured echo to reduce interference and improve measurement quality. Piezoelectric transducers are a mature technology that have not been fully applied to battery analysis, and many developments in this area may be inspired by simply reading through a manufacturer's catalog. For example, recent work has scanned focused transducers perpendicular to the battery surface to produce depth-resolved images of lithium (Li) plating.[26]

While piezoelectric transducers are the most common and accessible technology, others may improve on some of their shortcomings. Piezoelectric transducers either require coupling fluid or suffer high attenuation in air, which motivates using non-contact transducers such as EMATs. An EMAT uses a magnet and an electric coil, much like a traditional speaker. An alternating current (AC) excitation pulse at the ultrasound frequency is sent through the electric coil, generating magnetic eddy currents in the sample surface. These interact with the magnet via the Lorentz force to induce acoustic deformation. Further details can be found in other introductory texts.[38] While this avoids contact with the battery, an EMAT typically has a lower SNR and requires amplification and filtering to produce proper measurements.[39] EMATs have only recently

been applied to batteries,[40] but given the high demand in industry for non-contact metrology, it will likely see increased research interest in the future.

Laser ultrasound is similarly non-contact but uses differing physical processes for generation and detection. Ultrasound is generated by a high-power, short-duration laser pulse, which hits the battery and is partially absorbed. The absorbed light is quickly converted to heat, which causes thermal expansion and a pressure field propagating outward from the laser spot as an ultrasonic wave.[41] The ultrasound frequency is a function of the laser pulse width, which enables a broader generation bandwidth than is possible with a single piezoelectric transducer.[41] Detection is performed using a second laser by measuring its frequency or phase change after reflecting from the sample, typically using a resonator, etalon, or interferometer.[41] Like EMATs, laser ultrasound does not require a couplant to the battery. In addition, the ultrasound generation and detection area are constrained by the spot size of the lasers rather than the geometry of a piezoelectric crystal, which may enable significantly improved spatial resolution. Laser-based ultrasound has the shortcomings of variable coupling to samples (due to variation in optical absorption and thermal expansion coefficients) and more complex instrumentation. It also requires localized heating of the sample, which may induce thermal effects that are more difficult to analyze. While laser methods have tremendous promise, there have been limited applications in the battery field so far.[42,43] Since the generation and measurement use two different laser systems operating under different principles, it is possible to mix transducer types to leverage the advantages of various kinds. For example, a contact piezoelectric transducer generated guided waves within a battery that were mapped via non-contact laser doppler vibrometry.[44]

The final transducer type is the CMUT. A CMUT is a capacitor fabricated into a substrate with an air or vacuum dielectric cavity and a conductive membrane as the outward-facing plate of the capacitor. When the capacitor is charged, the plates experience an electrostatic attraction which causes the membrane to deflect inward until the mechanical elasticity of the membrane balances the attraction. To generate ultrasound, an AC signal is applied to the capacitor, which causes the membrane to vibrate at the AC frequency.[45] To detect ultrasound, the reverse process occurs: an acoustic wave causes the membrane to vibrate, which is measured as a change in the CMUT capacitance.[45] A key advantage of CMUT technology is its compatibility with silicon fabrication techniques, making it simple to create large arrays of CMUTs.[46] They also offer a much broader bandwidth in liquids than piezoelectric transducers.[45] Due to their small size and low cost, CMUTs have been proposed to be integrated directly into battery monitoring systems[47] but they remain underexplored in the battery literature.

Research within the field of ultrasonic transducers includes generating ultrahigh frequency (>100 MHz) acoustic waves,[48] transducers that can operate in extreme environments,[49] and flexible transducers.[50] These developments may be helpful to battery research, opening up new frontiers in spatial or time resolution with higher frequencies, *operando* studies in extremely high or low temperature conditions, or new form factors of transducers more suitable for integration into a BMS. Battery researchers should stay aware of these developments and identify opportunities for collaboration with ultrasound-focused labs.

Ultrasound Generation and Measurement Instrumentation

In order to perform a UT experiment, instrumentation is needed to generate and measure the electrical pulses from the transducers. We will discuss the hardware associated with piezoelectric transducers, though there is some overlap with the other transducer types. The generation side is usually handled by a pulser or arbitrary waveform generator, which sends a short duration, high voltage pulse to the transducer to cause it to generate the acoustic wave. Important factors to consider are the pulse width, pulse voltage, and pulse repetition frequency (PRF).

The pulse width determines the frequency of ultrasound generated. A standard pulser will send a single voltage pulse and produce a short duration ultrasonic wave with a Morlet wavelet-type shape. An alternative is a tone burst pulser, which generates a sinusoidal wave with a controllable number of periods. There are tradeoffs between the two: a tone burst contains more energy per pulse and has a better-defined frequency than a Morlet, whose short duration limits how well-defined its frequency can be due to tradeoffs inherent in the Fourier transform. On the other hand, tone burst pulses can suffer from near-field interference that is less of a concern than for shorter wavelets.[51] In general, tone burst pulses are preferred for air-coupled experiments whereas Morlets are used for most other applications.

The pulse voltage determines the pressure of a single ultrasonic wave. For piezoelectric transducers, greater voltage results in a greater displacement of the transducer, which causes each pulse to carry more power if pulse width is kept constant. Higher pulse voltage will improve SNR, but applying too much power per pulse can result in sample heating.

PRF is the rate that individual pulses are sent out from the pulsing transducers and determines how quickly data can be collected at a single measurement point. It is limited by the hardware and the rate of attenuation of the UT signal - a pulse must be fully attenuated before the next one can be sent in order to avoid ambiguity in interpreting the measurement. A typical PRF is on the order of 1-10 kHz. Depending on the intensity of the measured signal, multiple pulses may need to be averaged together to produce a sufficiently high SNR to detect features of interest. As a result, overall measurement rates for a UT experiment can range from low kilohertz (PRF limited) to single hertz (averaging thousands of samples). This sampling rate is much faster than even the fastest battery charging rates, meaning UT can provide hundreds to millions of individual measurements during a single charge-discharge cycle.

On the measurement side, data is usually recorded by an oscilloscope. The pulser and oscilloscope must be coordinated by a trigger in order to accurately measure the timing of the ultrasound moving through the sample. Amplifiers are often required for pulse-echo measurements to increase the signal intensity from the measuring transducer. In addition, an analog bandpass filter is sometimes applied to remove noise outside of the targeted frequency.

Ultrasound Signal Processing for Batteries

This section provides an overview of common UT metrics, their physical interpretations, and fundamental signal processing techniques used in battery research. By relating changes in recorded transducer voltage over time (directly proportional to acoustic pressure) to the underlying physics of wave propagation (Figure 3a), UT offers valuable insights into battery behavior. This is not an exhaustive review, but rather a guide to help readers interpret UT-based battery studies. Corresponding algorithms are detailed in Supplementary Section S1.

SA (**Figure 3b**) is the magnitude of the received acoustic wave, and its physical interpretation is mode dependent. In through-transmission, decreasing SA indicates higher acoustic impedance mismatches, where signal is reduced. For pulse-echo mode, decreased SA of signal with limited penetration depth indicates a lower acoustic impedance mismatch (more transmission, less reflection). In contrast, decreasing SA for the first echo, which has propagated through the entire cell and reflected, means a higher impedance mismatch, similar to through-transmission. Attenuation can also decrease SA in all modes. Thai metric is particularly valuable for defect detection, as the formation of new interfaces directly affects the SA.

Time-of-flight (ToF) (**Figure 3b**) is the propagation time of the wave. This metric is directly related to the speed of sound and effective material properties through the interrogated region (Eqn. 9).

$$ToF = \frac{x}{c} = \sqrt{\frac{x\rho_A}{E_{eff}}} \quad (9)$$

Here, x is the acoustic path length, and ρ_A is the effective areal density. In through-transmission, x is defined as the distance between the transducers. This is constant in a constant volume system (ex: stack pressure restricts volume expansion), but variable if the transducers are allowed to move with cell expansion and contraction. For pulse-echo systems, x is twice the penetration depth of the reflected signal. Typically, ρ_A is considered a constant since batteries are closed systems with a constant total mass (m), and the area (A) under investigation is constant. Note that a fundamental assumption here is that m in the acoustic path is essentially constant, meaning volume changes are primarily occurring in the direction of the acoustic path, and therefore addressed by changes in x. ToF is often used to track material property changes and degradation, as cell volume and elastic properties change with lithiation, delithiation and degradation.

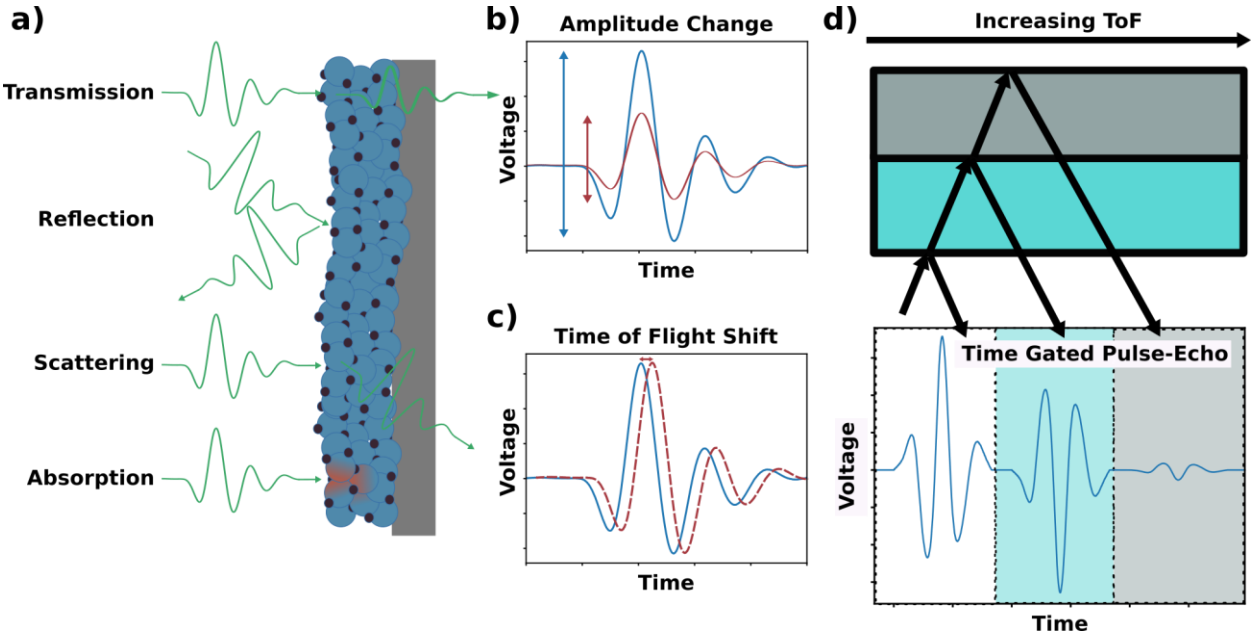

Figure 3. a) Commonly encountered interactions between an acoustic wave and a material layer within a battery. Note that scattering and absorption both contribute to attenuation. Analysis is often performed by comparing the amplitude (b) or time of flight (c) between two cells with manufacturing variations or as a single cell undergoes some physical process. (d) Schematic illustrating an acoustic pulse propagating through a sample and being reflected, and the corresponding pulse-echo signal that would be measured. By dividing the signal into sections (time gating), each signal can be assigned a depth within the sample. Note that it is possible for pulses to reflect off of multiple interfaces before being measured, which makes depth profiling by time gating an inherently approximate method.

Most UT battery papers focus on ToF shift, rather than absolute ToF. This involves calculating the change in ToF relative to a reference waveform, often one taken at the top or bottom of charge. On the other hand, absolute ToF, the first break or wave arrival time, can allow for direct calculations of E_{eff}. This involves knowledge of m and A, which can be measured easily if assumed constant, and x, which can be set continuous if the system volume is fixed, or measured *operando* using additional techniques.[7] Absolute ToF algorithms are typically more sensitive to noise than ToF shift algorithms, which can lead to reduced accuracy. To mitigate this, an absolute ToF algorithm can be applied only to the reference waveform, while

a ToF shift algorithm is used to compute the relative ToF change with respect to that reference. This combined approach reduces noise sensitivity and provides a more accurate estimate of the absolute ToF evolution.

Recent studies have begun to explore damping in batteries, defining it either as the ratio of received to incident waveforms[52] or as the logarithmic ratio of successive echo amplitudes.[53] Increased damping generally arises from greater absorption and scattering and may differentiate states of matter, with more weakly packed phases (e.g., liquids) exhibiting higher damping than solids. Despite this, damping remains relatively underexplored in the UT battery literature. One potential challenge is that evolving interfaces during cycling could alter waveform shapes, complicating the interpretation of waveform ratios and peaks. Nevertheless, damping may provide information similar to amplitude while normalizing for system-level variations, highlighting its potential for improved cell-to-cell comparisons and warranting further investigation.

Frequency-domain analysis involves a unique set of metrics and considerations. System variations may affect the propagation of different frequency components in the signal. For example, the development of more microstructures, defects, and gassing in batteries can hinder the ability of high frequencies to pass through the system.[6] Of particular interest is resonant analysis. Batteries, with their layered, quasi-periodic structures, exhibit characteristic acoustic resonances. These resonances arise from constructive interference of ultrasound waves reflecting within the repeating layers. As such, analyzing resonant frequency amplitude can provide detailed information about the battery's internal structure and changes occurring within. For instance, defects that disrupt the periodicity of the layered structure, such as delamination or cracking, will weaken or shift the resonant frequencies. Resonant frequency amplitude can be a more sensitive indicator of subtle structural changes than SA in the time domain.[24]

Waveforms can be decomposed to provide richer insight into specific battery elements. Gating divides the signal into time-bounded segments, analyzing each independently in both time and frequency domains (**Figure 3d**).This can eliminate unnecessary signal components (e.g. front-wall reflections from cell packaging that do not contain information about the internal cell) and isolate specific signal regions (first echo, internal cell reflections, etc.).[21,54] Correlating time-trace regions with cell depth can allow for depth-resolved analysis. Combined with SAM, this can provide a 3D picture of the cell.[55] Wavelet decomposition has also been used to isolate reflections.[22] Notably, these techniques are more relevant in reflection mode, where the waveforms peaks can be assigned to specific regions, rather than transmission, where they represent the bulk.

Signal quality is crucial to UT analysis. Outside of experimental and hardware-based improvements, post-processing methods can improve signal quality by reducing noise and highlighting features of interest. Upsampling by interpolating points within each individual waveform can improve resolution by artificially increasing the sampling rate. This is useful for initial wave break and cross-correlation calculations, especially for smaller systems such as single-layer pouch cells where cell variation has a negligible effect on the acoustic signal.[7] SNR issues can be addressed using waveform averaging and smoothing techniques, such as convolution, though these come at the expense of pulse time and waveform feature resolution. Post-process bandpass filtering can remove frequencies which may result from electromagnetic interference or unwanted reflections. The appropriate bandpass filters are determined by studying the present frequencies. Power spectral density (PSD) shows the signal power distribution across frequencies.[56] Alternatively, continuous wavelet transforms (CWT) or empirical mode decomposition (EMD) can decompose the waveform and isolate noise.[21,57]

Ultrasound Applications to Battery Research

The basis of applying UT to batteries lies in the chemomechanical changes that the cell undergoes during cycling, degradation, and failure. In this section, we discuss research findings for battery applications in UT. In addition to providing an overview of some specific findings of interest, we highlight commonalities across studies on ultrasound responses as they relate to particular battery phenomena and discuss the physical reason for these trends. Unless otherwise noted, the systems discussed here are multilayered Li-ion pouch cells with liquid electrolytes and the acoustic interrogation is conducted with longitudinal bulk waves, due to the prevalence of these factors in UT literature.

SoC/SoH Tracking

A significant application of UT is tracking battery SoC and state of health (SoH). This analysis operates on the principle that electrodes undergo repeatable material changes upon lithiation and delithiation. Some SoC-dependent material properties relevant to acoustic response are highlighted in **Table 3**. We note that E (Young's modulus) of the individual materials is different from, but directly related to, E_{eff} (effective elastic modulus) of an electrode, as discussed in Eqn. 8. The combined effect of these electrodes results in a repeatable intracycle acoustic response. Due to their commercial relevance, numerous studies have investigated SoC variations in cells with graphite and commonly used positive electrodes such as LCO, lithium nickel manganese cobalt oxide (NMC), and lithium iron phosphate (LFP). Linking physical changes in the electrodes during cycling to UT metrics (**Figure 4**) makes an informative case study for interpreting UT studies.

ToF is common in SoC tracking because the solid electrode particles have larger E values than the liquid components, meaning material changes strongly influence the ToF in these electrodes.[58] During charge, lithiation causes graphite E to increase and ρ to decrease, resulting in a ToF decrease, while delithiation during discharge causes a ToF increase. This was confirmed experimentally by using an extra-thick separator to isolate the graphite acoustic response.[59] In contrast, during battery charge or delithiation of the positive electrode, LCO and NMC tend to demonstrate a decrease in Young's modulus and density. At the same time LFP is reported to have an increase in both values. The same study that isolated graphite effects found LFP showed an increase in ToF during charge, likely because the ρ increase dominated.[59] To our knowledge, no reports have isolated the ToF change for the layered oxides NMC and LCO, but their Young's modulus and density changes would have contradicting effects on ToF. Interestingly, UT studies using through-transmission, pulse-echo, and pitch-catch on NMC or LCO systems have found ToF decreases on charge and increases on discharge for these systems. The same was observed in pulse-echo on LFP systems.[59] Overall, this suggests that graphite dominates the acoustic response.[15,17,22,60,61] While there may be some contributions from the decreasing density of graphite and NMC or LCO during charge, most studies attribute this to the three-fold increase in Young's modulus graphite experiences during lithiation (charge), which is more significant than the positive electrode density changes and modulus change.[15,17,61–63] This is further exacerbated by the larger volume of the graphite over the positive electrode in commercial cells to achieve capacity matching.[17,62]

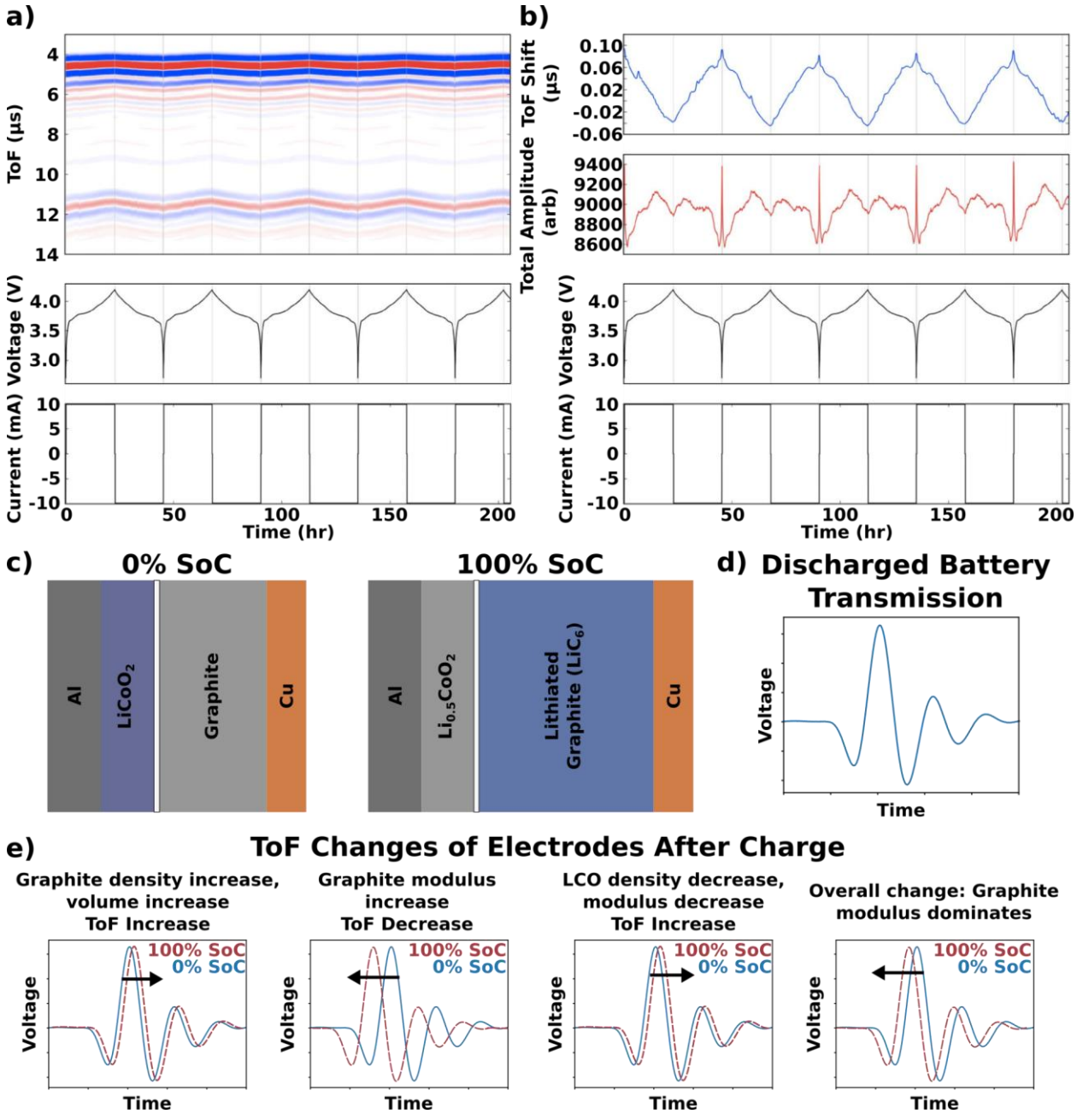

Figure 4. ToF changes in an LCO-graphite cell during cycling. a) Representative ultrasonic signal during cycling for several cycles of a LCO pouch cell at a C/20 charge/discharge rate. The TOF heat map shows maximum and minimum waveform amplitudes in red and blue respectively. b) The same ultrasonic data reduced to a time of flight and amplitude metric. The blue and red lines represent the single TOF shift and amplitude measures respectively. c) Schematic of the material layers in the cell in the discharged (0 % SoC) and charged (100 % SoC) state. Note the significant change in graphite volume after charging (lithiation). d) A reference ultrasonic transmission waveform through the discharged state. e) Effects on the ToF versus the discharged state for each material change in isolation and the observed overall change. Based on experimental data, the change in graphite E_{eff} dominates the ToF change during cycling. Detailed discussion of the relative magnitude of each of these effects can be found in Davies et al.[17] Panel a) and b) adapted from [17]. Copyright 2017 The Electrochemical Society. Reproduced by permission of IOP Publishing Ltd.

SA exhibits SoC dependence. In LCO and NMC || graphite cells, SA increases during charge and decreases during discharge for transmission, internal reflections, and back-wall reflections, with similar trends observed in frequency-domain transmission amplitude.[17,24,26,62] When graphite contributions are isolated, SA also increases upon charge, reinforcing the conclusion that graphite dominates the acoustic response.[59] This behavior is commonly attributed to increased stiffness and reduced porosity during lithiation, which lowers absorption and scattering and thus reduces attenuation.[15,24] Similar trends have been reported for LFP || graphite cells, though attributed instead to evolving electrode acoustic impedance matching during charge.[25] However, this interpretation implies opposite SA responses for transmitted and internally reflected signals, which contrasts with the commonly observed SA increase across all signals. Future work should therefore jointly analyze internal reflections and transmitted signals to clarify the impact of impedance effects versus absorption and scattering contributions. More broadly, SoC/SoH tracking using ToF and SA would benefit from isolating electrode-specific acoustic contributions. This could be achieved through system modifications, such as using an extra-thick separator, or by leveraging "zero-strain" materials like lithium titanate oxide (LTO), which undergo minimal mechanical change and therefore have reduced acoustic impact.[64]

Table 3. Young's modulus and density of current collectors, separators, and electrode active materials at 0 % and 100 % SoC. We again note that there is variation in reported material properties across studies.

Material	**E @ 0 % SoC (GPa)**	**E @ 100 % SoC (GPa)**	**ρ @ 0 % SoC (g/cm^3)**	**ρ @ 100 % SoC (g/cm^3)**
Graphite ($C_6 \rightarrow LiC_6$)	32[63]	109[63]	2.26[13]	2.20[13]
a-Si ($Si \rightarrow Li_{3.75}Si$)	92[65]-105[66]	12[65]-41[66]	2.3[66]	1.18[67]
Li	-	2[68]-8[66]	-	0.53[67]
LCO ($Li_{0.5}CoO_2 \rightarrow CoO_2$)	178±5[16]	89±3[16]	4.46[17]	4.9[17]
NMC532 ($LiNi_{0.5}Mn_{0.3}Co_{0.2}O_2 \rightarrow Li_{0.5}Ni_{0.5}Mn_{0.3}Co_{0.2}O_2$)	145[68]	115[68]	4.76[69]	3.57[a]
LTO ($LiTi_2O_4 \rightarrow Li_2Ti_2O_4$)	209[70]	181[70]	3.74[71,72]	3.74[b]

LFP ($LiFePO_4 \rightarrow FePO_4$)	123.8[73]	125[73]	3.59[c]	3.75[c]
Cu	124 ± 0.7[18]	-	8.93[19]	-
Al	69[19]	-	2.71[19]	-
Celgard	0.55[14]	-	0.75[14]	-

[a]Estimated based on the predicted volume change of -2.5 %[69], noting this assumes negligible volume change.
[b]LTO is largely considered a "zero-strain" material, exhibiting negligible volume changes (0.2 %). As such, density is typically considered constant.[64]
[c]Calculated using lattice and structural information from Maxisch and Ceder 2006.[73]

SoC analysis via UT has also been investigated for next-generation chemistries. Anode-free Li metal systems charge resulting in a ToF increase, contrary to the graphite trend.[74,75] This was attributed to the Li metal having a smaller *E* than the layered oxide electrodes, reducing the bulk effective stiffness of the cell. Furthermore, plating Li metal increases volume, which increases the acoustic path length. Silicon (Si) also exhibited a ToF increase on charge, this time attributed to its elastic softening and a 300 % volume expansion on lithiation.[66,76] A 30:53 ratio Si-graphite composite electrode showed similar behavior to other graphite electrodes.[77] The dominant weight fraction of graphite justified this. Given the commercial relevance of Si-graphite composites and the uniquely significant volume expansion of Si, further work should investigate the variable acoustic response of these systems. Outside of ToF, SA demonstrated clear trends in Si systems with solid-state electrolytes. The volume expansion of the Si particles reduced the porosity of the overall system, increasing SA with lithiation and decreasing SA with delithiation.[76] Here, UT is uniquely suited to study the critical mechanical variations within this system.

Intercycle acoustic variation over cycle life provides insight into SoH based on the irreversible material changes in the battery. In anode-free Li metal systems, a ToF increase with cycling was attributed to the buildup of dead Li decreasing cell stiffness and increasing volume.[74] Similarly, an overall ToF increase in Si and Si-graphite systems was attributed to permanent volume expansion and softening of irreversibly lithiated Si particles.[76,77] In both cases, the increasing ToF was also hypothesized to result from the buildup of electrolyte degradation products called the solid-electrolyte interphase (SEI).[74,76,77] Li and Si demonstrate a more unstable SEI compared to graphite, particularly due to their greater mechanical change during cycling. As the SEI is insufficiently passivated against further electrolyte decomposition, degradation products accumulate. The resulting softening and volume increase is suggested to permanently increase ToF.[77] Results for layered oxide || graphite systems have varied between studies, with some citing decreased ToF from increasing density due to SEI buildup.[15,78] In contrast, others have noted an increase in ToF which was attributed to softening with degradation.[79,80] Results for SA are less often reported. Some studies have pointed out a "break-in" period where SA increases during initial cycles due to increased electrolyte

penetration, resulting in decreased acoustic impedance.[58] With aging, some studies have found decreasing SA while others have found an increase.[15,78,80]

The lack of consensus across these studies likely arises from differences in degradation pathways contributing to SoH decline, which generate distinct acoustic responses that may also depend on the UT mode employed. Slight differences in cell chemistries, formats, and cycling protocols also yield unique degradation modes. Still, it has been repeatedly observed that acoustic trends do correlate with SoH, opening up the possibility for SoH tracking via UT if the relationship between specific degradation modes and acoustic response for different UT modes can be better defined. One way this can be achieved is through rigorously controlled studies in which cell chemistry, format, and cycling conditions are carefully managed, allowing specific degradation pathways to be repeatably linked to acoustic signatures and validated through *ex situ* analysis.

In addition to these general trends, intracycle analysis can provide information on specific mechanisms during cycling. Some studies have attributed intracycle trends to the development of stress in electrodes. Following ToF changes associated with charge and discharge, a relaxation of ToF was observed during constant voltage holds and open circuit voltage (OCV), suggesting that UT is sensitive to the relaxation of the Li gradients.[60,81] These changes were observed to become more significant with increasing C-rate, which is expected given that Li gradients within the electrodes are more significant under these conditions. Additionally, SA changes have been attributed to impedance changes resulting from Li concentration gradients between the electrode and electrolyte.[58] Some studies have hypothesized that significant SA and ToF changes at the top and bottom of charge are associated with layered oxide phase transformations.[15,17,62] Notably though, increases in impedance at the top and bottom of charge also generate heat, which scales proportionally with C-rate. As will be discussed, it is essential to decouple the effects of internal temperature changes on acoustic signals from SoC-dependent variation to validate the observations of stress. Still, while the negative electrode typically dominates general trends, this motivates using intracycle trends to observe positive electrode behaviors. For example, Sun et al. detected liquid-to-solid phase transformations in sulfur (S) electrodes using intracycle ToF and damping.[53] While the overall trend was dominated Li metal, as confirmed by *operando* pressure measurements, the nonlinear intracycle trends were attributed to the S electrode based on the linear behavior of Li plating and stripping.[53] Variations in these intracycle trends throughout cycle life can provide greater insight into degradation modes.

A handful of studies have applied UT to track SoC/SoH in 18650 cells, specifically nickel cobalt aluminum oxide (NCA) || graphite[62,82] and NMC || graphite.[83,84] The cylindrical geometry significantly increases the complexity of the waveform by increasing scattering and introducing circumferential waveform propagation around the casing.[83] Overall ToF trends with SoC still show good agreement with pouch systems, but SA trends show greater variability between studies.[82] This variability in SA is believed to be due to the unique interactions of jellyroll swelling and deformation in a constrained cylindrical environment, as well as the complexity of scattering between jellyrolled layers.[82–84] At this point, most cylindrical studies focus on correlative trends, with limited discussion of intracycle trends and their implications for evolving material properties. Future work should look to improving analysis through a better understanding of wave propagation in cylindrical formats and how constrained systems versus flexible pouch cells may affect trends. Different analysis metrics, such as those in the frequency-domain metrics may produce more meaningful results than time-resolved SA alone.[83] Furthermore, advanced UT setups, such as curved transducers, may improve signals and yield more repeatable results. Finally, existing studies use a range of frequencies from 100 kHz to 5 MHz, but the impact of frequency in these systems should be thoroughly investigated.

Acoustic models often complement SoC/SoH UT studies. This necessitates estimation of E_{eff} and ρ of the electrodes and separator. A first-pass estimate of these values is the weighted average of the material properties. Some representative values are shown in **Table 2**. Otherwise, some models have leveraged

models of granular materials, with methods such as Hashin-Shtrikman, Voight, and Reuss bounds.[7,17] The typical treatment of the layered battery structure as an isotropic, homogenous solid is often achieved via Backus averaging, which takes the harmonic average of the effective material properties of n individual layers ($M_{eff,i}$) to calculate the effective material property of the cell ($M_{eff,cell}$) (Eqn. 9):[7]

$$M_{eff,cell} = n \times \left(\sum_{i=0}^{n} \frac{1}{M_{eff,i}}\right)^{-1} \quad (10)$$

This estimation results in wave speed predictions that are up to 20 % faster than those that were experimentally observed.[17,62] Given the lack of reported and validated viscoelastic values for involved materials, Ladpli, Kopsaftopoulos, and Chang 2018[15] further assumed all materials to be elastic, which would notably remove absorption effects from the model. With these assumptions, these particular studies were able to generate models that mimicked the general relative trends in ToF and SA for layered oxide || graphite systems. On the other hand, these models failed to capture intracycle trends accurately. Improved models of granular materials may address this, which is an ongoing research area, and better estimations of material properties.[2,15] The Biot model for fluid-saturated porous media is commonly discussed in this context. While it has been found to accurately portray the separator material,[85] applications to the electrodes have shown inconsistencies with experimental findings. Some studies have instead used the slurry model, positing that the mechanical behavior of the electrode systems is more similar to a dense liquid than a porous fluid-filled solid. Intracycle SA trends were also captured using the Dualfoil model to capture Li-ion concentration gradients in the electrode and electrolytes during a cycle.[58] Furthermore, replacing Backus averaging with layer-by-layer modelling can improve model accuracy, particularly by incorporating considerations of dispersion at layer interfaces.[54,86] Some works have leveraged more complex mathematical models using the transfer matrix method to model layer stratification.[54] Advancing modeling of ultrasound behavior in batteries can not only improve the interpretation of UT results, can also enable additional UT capabilities such as visualizing the internal structures of batteries without *a priori* knowledge and better deconvolution of individual material contributions to the resulting signal.

One of the challenges of SoC/SoH tracking and other UT applications is the sensitivity of acoustic propagation to temperature. Since acoustic propagation occurs via vibrational energy traveling between particles in the system, temperature directly affects material properties and the resulting acoustic signals. Heat generated in cells due to impedance (Joule heating) and exothermic parasitic reactions can increase temperature even under standard cycling protocols. UT analysis on OCV cells undergoing temperature fluctuations within the manufacturer-specified range has observed an increase in ToF and a decrease in SA with rising temperature, attributing this to thermal expansion of the cell increasing path length and, consequently, attenuation.[81] It has also been suggested that decreasing viscosity can increase attenuation. Although studies have observed SoC to dominate the acoustic signal, temperature can still affect results. Many battery studies have addressed this using low C-rates such that Joule heating contributions are minimal. Otherwise, temperature compensation is needed. One way this can be achieved is through the experimental collection of acoustic metrics versus temperature. This must be done at different SoCs to account for the SoC-dependent material properties.[81] Then, with knowledge of the cell temperature from a thermistor measurement, the temperature component of the acoustic signal can be subtracted, resulting in acoustic trends that are solely a result of SoC.[81] Still, improving experimental design and algorithms for temperature compensation, and developing more accurate methods for cell temperature measurements, is valuable future work.

While UT has been applied across a range of C-rates, most studies favor relatively slow cycling (C/20–C/10).[82] This minimizes, though does not fully remove, Joule heating impacts depending on chemistry and SoH. Still, acoustic response has been shown to vary with C-rate even when temperature effects are removed. Variations in intracycle acoustic trends have emerged when comparing slow C-rates (~C/10) to faster C-rates (~1C). These may result from a variety of factors, including different stress-strain behavior

and C-rate-dependent material properties, such as current-dependent graphite staging.[81,87] One study even observed different overall SA trends with C-rate.[82] These factors must be carefully considered when comparing UT results across SoC studies, particularly when moving toward higher, more realistic C-rates. Despite this complexity, UT studies under drive-cycle conditions with rapidly varying currents have shown promising SoC tracking, with temperature-compensated ToF maintaining reasonable predictive capability despite some variation in intracycle behavior.[81,87] Further work is needed to extend these findings across different chemistries and SoH.

A significant application of SoC/SoH tracking from a research and development perspective is gaining insight into degradation modes to drive forward new chemistries. Bommier et al.[77] used intracycle trends to distinguish silicon and graphite behaviors, and with this were able to attribute observed capacity losses to primarily passivation and irreversible lithiation of the Si particles. Chang et al.[74] compared dQ/dV analysis to dE/dV analysis. They found that initial behavior followed a generally linear dE/dV trend, which tracks the expected behavior of ideal Li plating and stripping. With cycling progression, they correlated deviations from linearity with nonideal behavior, such as mossy Li plating, incomplete Li stripping, and SEI buildup. This analysis was used to gain further insight into the impact of both electrolyte and formation rate on the chemomechanical stability.

From a field-deployed perspective, UT also has the potential to improve SoH/SoH tracking and prediction through integration with existing BMSs. Current SoC estimation methods rely on voltage tracking and Coulomb counting, which can be inaccurate. Voltage is affected by voltage fade, impedance changes, and the dependence of overpotentials on current, while Coulomb counting can be affected by capacity loss in the cell or environmental conditions.[17] The addition of the chemomechanical insights provided by acoustics into SoC estimations, typically made by BMS systems, can improve the accuracy of these estimations. Davies et al.[17] demonstrated a machine-learning model for LCO || graphite. While the use of ToF and amplitude alone led to slight improvements in SoC estimation over voltage alone (2.3 % vs. 3 %), the combination of voltage, ToF, and amplitude led to a ~1 % error. This suggests integrating acoustic data alongside electrochemical information can improve prediction capabilities. This improvement was even more drastic for LFP (6 % to 1 %), where the flat voltage profile and voltage hysteresis generally make SoC estimation more difficult. Similar results were found even when the model trained on healthy cells was extended to one damaged by overcharging. Owen et al.[81] further used temperature-compensated ToF to predict SoC under drive cycle conditions using fitting of collected SoC versus ToF data, demonstrating the applicability of this method under conditions more realistic for field-deployed batteries.[81] This can be further extended to SoH determination. In the same work, Davies et al.[17] showed significant promise of machine learning with combined acoustic and electrochemical insights for predicting the SoH of cells.

This is valuable for field-deployed batteries, which may not be able to undergo electrochemical tests during real-time use. While laboratory results have been promising, it should be noted that the collection of representative datasets determines prediction accuracy to generate accurate SoC vs. acoustic parameter relationships. Collecting this data will likely be a challenge given the wide variety of batteries used in field-deployed applications, and the numerous cycling protocols used. Furthermore, extensive data on cells with varying SoH will be necessary to retain prediction accuracy throughout battery life. The development of rich data sets for individual battery chemistries and formats, and improved knowledge of cell-to-cell variation within batches, can allow for correlations between acoustic information and SoH with limited *a priori* knowledge of the particular cell.[15] There is also the potential for the insights generated from acoustics to show degradation before it affects electrochemical performance. For example, Chang et al.[74] showed that an effective stiffness decrease in an anode-free cell happened before any electrochemical change was seen (within 30 cycles). Extrapolating this further, it is possible that this chemomechanical variation can be an indicator of future failure but implementing this realistically will require large data sets and advanced algorithms.

Gas Detection

Another wide-ranging application of UT is the detection of gas in cells. In this section, we discuss gas in the context of both dry regions in the cell and gas bubbles forming byproducts of side reactions. Ultrasound is particularly sensitive to this due to the high acoustic impedance mismatch between gas and condensed matter. At these interfaces, ultrasound waves experience greater reflection and dispersion and, consequently, less transmission. Through-transmission is therefore very sensitive to gas because even small amounts of gas trapped between electrode layers can significantly hinder the ability of the waveforms to propagate through the entire system. This results in signal attenuation. In pulse-echo, this is dependent on the signal penetration depth. When only surface layers are examined, such as in cases with high-frequency transducers with limited penetration depths, the signal increases due to increased reflections on the gas-condensed matter interface. Attenuation increases with increasing penetration depth, as the ability for the signal to transmit past the initial gas layer is hindered. As a result, the first echo tends to exhibit significant signal attenuation with gassing, similar to the through-transmission results.[88,89] While ToF also shows an increase with gas formation, the signal attenuation is a more evident and detectable change and hinders the extraction of other acoustic metrics by increasing SNR. As such, most gassing studies focus on SA or signal energy. The effects of gas formation on UT signals are summarized in **Figure 5a**.

The sensitivity of ultrasound to solid or liquid to gas interfaces has been used to study the electrolyte wetting process. Battery electrodes are porous, and it takes a significant amount of time for the electrolyte to displace gas in the film. Acoustically, this results in highly reflective solid-gas interfaces being replaced by transmissive solid-liquid interfaces, causing the intensity of the transmission signal to increase and pulse-echo signal to decrease. This process has been directly observed by SAM (**Figure 5b)**, though only for a few electrode and electrolyte combinations.[20,35,90] The wetting process is a significant time bottleneck in battery production, so nondestructive monitoring represents a major avenue of optimization and further research.[91]

This analysis has also been used to detect electrolyte saturation/dryout and gassing during precharge, formation, and aging. Deng et al.[90] observed signal attenuation while cycling NMC532 || graphite and LFP||graphite cells. This was attributed to gassing and electrode swelling which resulted in insufficient wetting, both consequences of degradation modes caused by continuous cycling. These were further correlated with capacity losses, pointing to UT's value for identifying specific failure mechanisms in aging cells. A similar result was found by Louli et al.[92] in anode-free Li metal cells paired with NMC532. Here, more signal attenuation was observed in the system with lower stack pressure than with higher stack pressure. X-ray tomography observed more porous Li plating in the low stack pressure configuration, suggesting the attenuation results from electrolyte depletion. Notably, both studies utilized spatially-resolved ultrasound. This was beneficial as it revealed inhomogeneities and allowed for a better comparison of the degree of dryout throughout the cell area. In contrast, Bommier et al.[77] observed significant attenuation in stationary transmission data during the initial cycles of Si-graphite electrodes, attributing this to gaseous byproducts resulting from the formation of the initial SEI. Such a finding suggests potential for using UT as a means for rapidly identifying incomplete formation and other acute events that can yield gas. In addition to the SoH metrics described previously, electrolyte dryout and gassing analysis are other ways to extend UT for long-term stability evaluation.

A similar application is the evaluation of interfacial contact in solid-state batteries. Poor contact between the electrode and the solid electrolyte results in small gas-filled pores, which results in transmission signal attenuation. Studies have leveraged spatially-resolved ultrasound as a means of observing contact heterogeneities, differentiating between poor contact and active gas formation, and studying the evolution of interfacial contact with cycling.[93,94] This method has proven useful for evaluating methods for improving interfacial stability.

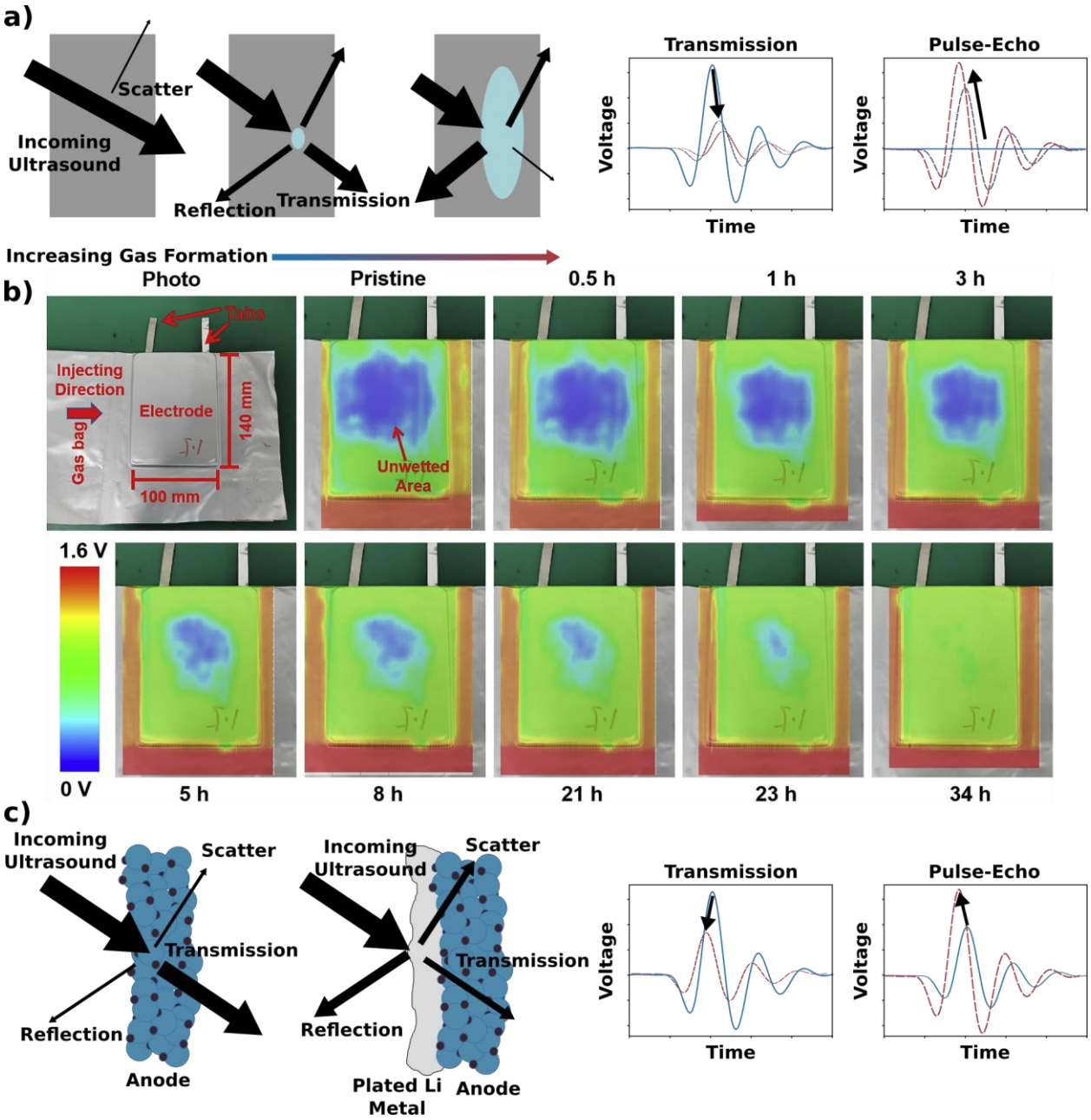

Figure 5. a) Changes in ultrasound upon gas formation. Transmission shows a decrease in amplitude and simultaneous increase in ToF. In pulse-echo mode, formation of bubbles will cause new features to appear that will grow in amplitude and decrease in ToF as the bubbles get larger. b) Electrolyte wetting process of an LFP || graphite pouch cell. SAM images are overlaid with photos of the cell, with the color bar indicating the SA. An increase in SA accompanies the electrolyte displacing gas, with 34 hours required for uniform wetting. c) Changes in ultrasound upon Li plating. A layer of Li will add a new reflecting interface with a higher speed of sound than the electrolyte it displaces. As a result, transmitted SA and ToF increase while pulse-echo will arrive sooner and may have a higher SA if the impedance mismatch between electrolyte and Li is greater than that of electrolyte and electrode. Panel b) reproduced with permission from [90]. Copyright 2020 Elsevier.

One of the significant challenges of gas analysis via UT is quantification. The presence and formation of gas and dry regions in cells are generally localized and develop stochastically. Studies that use only one or

a few transducers may miss instances of gas outside the acoustic path. Gas which forms *operando* also travels through the cell, which can result in transient acoustic signatures.[77] This was addressed in some of the previously mentioned works with spatially-resolved acoustic scans which can capture the initial location and movement of gas. With a single transducer, or a pair of transducers, this measurement is still limited by the scan speed relative to the formation and movement of the gas. In contrast, transducer arrays can simultaneously cover a significant cell area, providing an instantaneous picture of gas formation. Still, techniques using a normally incident and received signal are limited to 2D quantification since ultrasound cannot penetrate through the initial gas interface. Work by Xu et al.[33] utilized FMC with a phased array to transmit and receive both normal and oblique waves. The total focusing method (TFM) was then applied, in which signals from all transmit–receive pairs are coherently summed at each imaging point to produce a focused intensity map. This multi-angle approach effectively "sees around" gas bubbles, enabling 3D imaging and quantitative measurement of bubble size across multiple layers. Notably, the implementation of these spatially resolved techniques, as well as the increased data overhead, increases system complexity and cost, while also limiting field-deployed use.

Lithium Plating

UT has also been leveraged to observe Li plating. Li plating occurs when Li-ion batteries cannot properly intercalate into the negative electrode, forming metallic Li on the surface. These deposits can lead to lost capacity, increased impedance, additional electrolyte reactions, and in some cases, internal short circuits. Li plating is associated with aging, nonuniform pressure, high charge rates, and low temperatures. The basis for UT analysis of Li plating is the different material properties of Li metal compared to the electrodes, resulting in a high acoustic impedance mismatch. Similar to gassing results, Li plating results in attenuation of through-transmission[95] signals and an increase in internal layer reflections.[26] Furthermore, the formation of Li metal has a significant effect on the speed of sound, with ToF increasing with Li plating due to its much smaller Young's modulus, and possible thickness increases. The expected changes to the UT signal are summarized in **Figure 5c**.

Spatially-resolved methods are of particular interest here to identify the location of Li plating. Using SAM with through-transmission, Chang and Steingart[95] attributed signal attenuation around the tabs which increased with cycling to Li plating. Using a 25 MHz transducer with SAM, Wasylowski et al.[26] observed the opposite trend in SA in regions where Li plating was induced using markers, attributing this result to increased reflections due to the higher impedance mismatch. Here, spatially-resolved data is helpful as Li plating results heterogeneously throughout the cell.

Relative quantification of Li metal plating has also been explored using UT analysis. Xu et al.[24] leveraged amplitude analysis in the frequency domain. They specifically showed that the amplitude of the resonance frequency (3.8 MHz) was more sensitive to Li plating than typical transmission frequencies (2.25 MHz) due to the effect of Li plating on the battery structure, and consequently the resonance behavior. With this, they showed that the differential amplitude decreased with a magnitude proportional to the amount of Li plating. Furthermore, Bommier et al.[96] found a statistically significant correlation between current rate, temperature, and ToF endpoint, defined as the difference between ToF at the end of charge between non-plating and plating conditions. Specifically, they found the ToF endpoint to increase with the magnitude of plating, as confirmed with *ex situ* methods. Li plating quantification also motivates increased acoustic accuracy through temperature decoupling. Meyer et al.[97] achieved this using an experimentally-derived relation between cell temperature during Li stripping and signal intensity. These works demonstrate the ability of amplitude and ToF to track Li plating, and show promise for this method as a more quantitative tool.

One of the challenges of detecting Li plating is decoupling its acoustic signature from gassing. These phenomena have similar effects on SA and ToF in both through-transmission and pulse-echo modes, and

Li plating often results in gas formation due to electrolyte reactions. Gassing may be assumed based on the transient effect on the acoustic signature, as gas bubbles travel out of the electrodes and into the gas pouch. Still, the absence of transience could be associated with either electrolyte dryout or Li plating.[77] Furthermore, Li plating is sometimes transient, as deposited Li metal can reintercalate into graphite.[24] Here, spatially-resolved methods can provide more insight into the movement of regions with changed acoustic properties. For example, Wasylowski et al.[26] showed that SAM scans of cells demonstrated static regions of increased reflection which correlated to Li plating, whereas gas would have shown dynamic, mobile regions. Furthermore, they observed gas pockets to visually form more distinct, homogenous regions of signal change, whereas Li plating showed more diffuse and heterogeneous regions of signal variation. Still, there is a need for more definitive and quantitative methods for decoupling these phenomena, especially as spatially-resolved methods are more challenging to implement.

Other Applications to Failure Analysis

Given the ability for UT to detect both overall degradation, as shown by SoH studies, and acute events such as gassing and Li plating, many studies have leveraged UT as a means for detecting battery failure under abuse conditions such as overcharge, overdischarge, and extreme temperature fluctuations. In addition to performance fade, such situations can trigger an uncontrolled chain of heat-generating reactions and events in the cell, sometimes resulting in thermal runaway (TR), which may cause battery fires and explosions. UT shows much promise in detecting some of the initial indicators of failure. In addition to being sensitive to chemomechanical variation, the *in situ* and *operando* capabilities are especially useful for evaluating realistic abuse scenarios, particularly during battery cycling.

A promising application of UT is internal temperature detection. The generation of internal heat from various phenomena including internal short circuits and electrolyte degradation is a clear indicator of cell failure. Although the initial source of this heat may be localized, it can lead to chain reactions that can eventually cause TR. As such, rapidly detecting abnormal heat flow is a vital prevention mechanism for TR. While temperature measurements are currently implemented in many BMS systems, these systems typically rely on external thermistors which measure the surface temperature. Unfortunately, these measurements can be inaccurate detectors of localized heat formation due to heat dispersion throughout the battery. Furthermore, the lag associated with heat flux to the sensor can make this a poor warning system. UT, on the other hand, is a powerful tool for detecting the internal cell environment. As mentioned, increasing cell temperature leads to thermal expansion and decreasing viscosity, increasing ToF and decreasing amplitude. ToF is particularly valuable due to its approximately linear correlation with temperature, whereas SA exhibits nonlinear behavior.[81,82] Quantitative internal temperature determination using UT requires independent knowledge of SoC to decouple SoC-dependent material property effects. A prior calibration using thermal cycling at multiple SoCs is necessary, since the effect of temperature on material properties varies with SoC.[81] This approach relies on high-precision SoC measurements and becomes increasingly challenging as cells degrade. While feasible at the laboratory scale, a more practical field-deployable application is the detection of abnormal internal temperature through deviations from expected acoustic behavior. Under externally applied heating conditions, significant increases in ToF were observed beyond the established baseline range before the onset of other failure indicators, including gas evolution or voltage change.[89] While this shows promise for early failure detection, future work should investigate the accuracy of these warnings with concurrent cycling and at varying SoH.

Outside of temperature increases, abuse conditions result in various mechanical changes within the cell which are acoustically detectable. For example, early stages of overcharge and overdischarge exhibit increases in stress on the electrodes which correlate with amplitude changes. In a study on SoC/SoH analysis, Davies et al.[17] correlated a spike in the amplitude at bottom of charge to significant structural evolution during overdischarge. More aggressive abuse conditions result in gas formation from electrolyte

degradation, side reactions, or electrolyte volatilization. These gassing events can also induce or be accompanied by electrode delamination, and expansion. These factors hinder signal propagation due to higher impedance mismatches and decreased interfacial contact. Studies leveraging through-transmission and pulse-echo have observed decreasing amplitude corresponding with the onset of degradation under abuse conditions. In contrast to through-transmission and pulse-echo, McGee et al.[98] saw an amplitude increase in their guided wave analysis, hypothesizing that this results from delamination yielding a thinner elastic wave guide. Other significant events leading up to TR, including changes in material properties and porosity, have a marked effect on the acoustic response. Failure progression has been shown to show a repeatable, staged effect on UT for graphite-containing systems with varying positive electrodes and form factors, showing promise for this method across numerous cases.[99]

Studies have also conducted more quantitative analyses on battery failures. McGee et al.[98] further noted a positive correlation between the rate of attenuation and hold temperature, showing that UT can detect failure severity. Chang et al.[100] monitored cells undergoing rapid temperature shifts within the manufacturer-specified temperature range, noting significant gassing. They expanded on this result, correlating the onset of attenuation to the magnitude of temperature change and finding an Arrhenius relationship which helped evaluate the temperature-dependence of Li plating-induced gassing. As mentioned previously, Bommier et al[96] also found a statistically significant correlation between ToF shift and the amount of Li plating. While these results must be qualified against larger sample sizes of cells, these preliminary results suggest that ultrasound results could be used to quantify battery failures.

Clearly, UT is a powerful tool for detecting abnormal battery behaviors. Implementation of UT failure detection algorithms into field-deployable BMSs, along with existing temperature and voltage measuring protocols, can enable early warning systems. Protocols can establish a "normal" acoustic range associated with material and temperature changes associated with standard cycling. Any deviations from this range, whether internal heating, gassing, Li plating, or another mode, would indicate a failure and trigger a warning. Furthermore, correlating specific acoustic responses to stages of failure, as well as acoustic metric magnitude changes with failure severity, allows for a hierarchical warning system.[99] For example, ToF deviations could trigger early warnings for internal heating, while signal attenuation could indicate gassing or Li plating at higher warning levels.[89,98] These levels can then inform BMS protocols for corrective action and emergency stops, potentially enabling recovery of normal battery cycling with minimal performance loss before catastrophic failure.[101]

Operando Techniques for Lab-Scale Battery Research

A significant advantage of UT is its flexible and straightforward hardware, which leaves room for other probes. Interpreting ultrasound data and extending its analysis to specific chemomechanical changes within a cell often requires a secondary method to confirm the hypothesis. Therefore, combined experimental approaches will be essential for improving the application of ultrasound to new chemistries and battery metrics. A list of *operando* techniques that have been used with ultrasound is shown in **Table 4**. Values in this table are rough orders of magnitude for the purposes of qualitative comparison and are often subject to tradeoffs i.e. increased spatial resolution at the cost of longer measurement time. This is not an exhaustive list and we refer the reader to other relevant reviews for more information on the range of specific techniques.[102–107] Our emphasis here is on the relation of other *operando* measurements to ultrasound both in the overlap in the information they provide and the possibility of directly integrating ultrasound in a multimodal measurement. The goal of such combined experiments is twofold: enable the use of fast, low-cost UT in an industrial context to provide similar insights to those gained from much more expensive and slow measurements, or to use UT in combination with other probes to gain information that is not accessible from either technique in isolation.

Table 4. *Operando* battery measurements that have been combined with UT

Measurement Technique	**Properties Measured**	**Improvement to UT Interpretation**	**Information Added to UT**	Time Resolution[a]	Spatial Resolution[a]	Instrument Accessibility	Contact	**Notes on combining with UT**	**Examples**
UT	Density, modulus, speed of sound	-	-	100 µs - 1s	10 µm - 1 mm spot size	Can be built for <$10,000. Commercial instruments also available	Depends on transducer type	-	-
Electroanalytic Methods	SoC, SoH, mass transport, wetting, electrochemical processes	Improve accuracy of SoC/SoH modeling	Spatial resolution of global measures (wetting, SoC, etc)	Seconds to hours depending on technique	Whole cell	High performance potentiostats are available in most battery labs	Electrical contact	Requires little to no modification	[20,108]
X-Ray Diffraction	Material structures	Relate structural changes to UT metrics (phase changes, etc)	More narrowly defined structural parameters enables calculation of additional properties from	1 s - 10 min	100 µm - 1 mm spot size	Typically requires synchrotron for *operando* measurement of commercial cells	No	*Operando* x-ray in commercial cells typically requires synchrotron radiation	[61]

			ultrasound						
X-Ray Computed Tomography	3D imaging	Higher spatial resolution imaging	UT is faster, more sensitive to gas formation and electrolyte dryout	1 ms - 1 hour	10 nm - 10 µm voxel size	Often available in shared facilities or specialized labs	No	Usually done sequentially rather than simultaneously	[109]
Nuclear Magnetic Resonance	Chemical environment (^{1}H, ^{7}Li, ^{13}C)	Related chemical changes to UT metrics (lithiation of electrodes, etc)	Related chemical and mechanical changes during cycling or failure	1 - 10 minute	Whole cell	Often available in shared facilities or specialized labs	No	Requires specially designed sample holders	[110]
Acoustic Emission (AE)	Sudden chemomechanical changes: cracking, gas formation	Active measurement versus passive monitoring	Early failure detection, health monitoring	Passive monitoring. Signals are on the order of µs	Whole cell. Spatial resolution possible with advanced setups	Similar to UT. Can be built for <$10,000	Depends on transducer type	Uses nearly identical instrumentation but cannot be performed simultaneously	[111]

Thermal Monitoring	Surface temperature	Temperature calibration	Early failure detection, health monitoring	1 ms - 1 s[b]	Diffraction limited (~1 μm) if coupled with microscopy[b]	Commercial IR cameras available for <$10,000	No for IR imaging. Other measurements may require contact	Requires little to no modification	[112,113]

[a]Values are presented as approximate orders of magnitude

[b]Ranges are for IR thermography. Other sensors will have different performance metrics

Combined approaches are necessary to improve the physical interpretation of ultrasound. Many studies establish a correlation between a battery property and an ultrasound metric (i.e. ToF changes with SoC), but secondary methods are needed to establish why this occurs. For this reason, multimodal experiments that combine more chemically insightful techniques with ultrasound are essential to developing the technique. Examples include X-ray diffraction (XRD) to identify the structural transitions responsible for acoustic signal changes during cycling[61] or solid-state magnetic resonance to characterize the Li - solid electrolyte interface.[110] Perhaps the most commonly used technique in this regard is X-ray computed tomography (CT), which is used to verify the structural interpretation of acoustic data.[33,34,88,109]

Ultrasound can provide complementary information to another *operando* technique. For example, electroanalytic techniques can provide whole-cell-level insights into battery behavior that can be spatially resolved using SAM. For instance, electrochemical impedance spectroscopy (EIS) and OCV can be measured simultaneously with SAM to track electrolyte wetting on a global and sub-mm scale.[20] UT can also provide a different mode of measuring the same properties. For example, acoustic emission (AE) uses similar instrumentation to passively 'listen' to the sample and measure acoustic waves emitted by various processes such as crack formation or gas generation.[114,115] AE and UT have been combined for enhanced early failure detection,[111] and given the similarities between the two techniques further developments along these lines are expected. Similarly, UT has been combined with infrared (IR) imaging to improve TR detection.[113] Other recent work has combined UT with IR imaging, X-Ray CT, and XRD to examine the impact of pouch cell orientations within an electric vehicle (EV) battery pack on their SoH.[112] This multi-technique approach is immensely valuable for fundamental battery science and improving ultrasound method analysis. Beyond those discussed here, many opportunities exist to combine other measurement techniques with ultrasound.

Measurement Techniques for Battery Component Manufacturing

While UT of finished batteries has been the focus of most academic work, there is demand in industry for nondestructive and fast testing of the electrode manufacturing and cell assembly steps before evaluating the finished product. Example measurements include evaluating electrode coating slurries for uniformity and rheology, monitoring thin film coating uniformity and detecting defects in coated electrodes, and checking the stacked electrodes' alignment and tab weld quality.[4,103,116,117] We will briefly discuss existing techniques for making these measurements and how ultrasound can provide complementary information. Particular emphasis is placed on fast, inline measurement in a production setting. For a more comprehensive

discussion of existing inline methods for battery manufacturing, we refer readers to several existing reviews.[4,116,117]

Consistent deposition of electrodes from a slurry requires maintaining a variety of metrics within tolerance. These include viscosity, particle size, uniformity, and solid content, typically measured via rheometer, laser sizing, and densimetry.[116] Ultrasound can measure many of these slurry metrics, though the analysis often requires assumptions about the other properties or extensive modeling.[118] For example, acoustic particle sizing measures the frequency-dependent acoustic attenuation and relates this to particle size by scattering theory, assuming other parameters such as viscosity are known.[119] Similarly, ultrasonic densimeters leverage the sensitivity of reflection at an interface to the slurry's acoustic impedance (and therefore ρ).[118,120] As a result, UT of a slurry could complement other methods, providing additional verification of measured properties or additional information that cannot be gained from one measurement alone. In addition, many of these techniques are fast and require small equipment footprints, making them amenable to inline integration for real-time monitoring of electrode slurries as they are deposited.[118,121]

Electrode fabrication includes several steps that require measurement. Determinations of critical parameters, including ρ and porosity, are made with methods including optical interferometry for film thickness, beta gauges for mass loading, and computer vision for surface quality.[116] Other emerging techniques that may be used in electrode measurements include THz imaging[122] and spectroscopic ellipsometry.[123,124] Ultrasound can complement these techniques as ToF and attenuation can be related to the film density and thickness with certain assumptions. Thus far, UT has been used to monitor the electrode drying process,[125] calendering,[126,127] and defects in electrode films.[127] More advanced models may be able to directly calculate from ultrasound data a film's porosity and tortuosity,[2] characterize density gradients and binder migration within a film, or detect subsurface cracks and delamination.

Cell assembly involves stacking electrodes, welding tabs, and electrolyte filling.[4] The stacking step requires precise alignment of the electrodes and separator in order to maximize active material use and avoid shorts. Evaluating the stacking is typically done visually, with internal issues (misfolds, damaged electrodes, etc) only becoming apparent during later formation steps. There is interest in identifying these stacking errors earlier using nondestructive imaging techniques such as X-Ray CT,[128] magnetic resonance,[129] or by UT.[34,55] Extracting detailed structural information from complex acoustic waveforms is an active area of research.[22,130] After stacking, there is need for further development in NDE of the tab welds. This is a challenge for existing methods because the tabs are extremely thin (~10 μm) and buried within the battery stack.[4] Whether ultrasound could solve this challenge is still an open research challenge.[131–133] After stacking and welding, the electrode assembly is inserted into packaging and electrolyte is added. This is followed by a wetting and pre-charge step, formation, and then degassing, all of which can be monitored with UT.[134]

Challenges and Opportunities in Scaling to Industrial Manufacturing

Despite the promise of UT highlighted in the previous sections, widespread commercial adoption remains elusive. Industrial-scale pilot trials confirm UT's potential as an attractive non-destructive option for safeguarding high-value battery components and inspecting work-in-progress and assembled cells for quality,, as it interrogates their internal structure without exposing materials or operators to ionizing radiation.[135] Yet, the same evaluations expose several barriers that currently prevent UT from serving as a front-line, 100 % inline inspection method. In this section, we combine the perspective of a company focused on ultrasound instrumentation commercialization and that of a large automotive manufacturer to examine remaining barriers to adoption and highlight important areas for improvement.

Transferring technologies demonstrated in laboratory environments to production presents a significant challenge due to the scale, speed, and sensitivity required.[128] Battery cell plant capacities in the tens of GWh[136] and cell capacities around 100 Ah[137] are publicly disclosed parameters. From an example electric vehicle original equipment manufacturer (OEM), a calculation of the maximum daily cell plant output in capacity and cells across all of its lines follows (Eqns. 11 and 12).

$$\frac{400\ GWh}{Year} \times \frac{Year}{50\ Weeks} \times \frac{Week}{7\ Days} = 114\ \frac{MWh}{Day} \quad (11)$$

$$114\ \frac{MWh}{Day} \times \frac{1}{3.5\ V} \times \frac{Cell}{100\ Ah} = 327{,}000\ \frac{Cells}{Day} \quad (12)$$

To achieve this scale, the coating, drying, and calendaring stages of cell manufacturing lines typically operate at 50 to 100 meters per minute without interruption,[4] a significant speed increase over doctor blade coating (1-5 m/min) found in many academic labs[138,139] or pilot line coaters (5-10 m/min) found in many scale up test facilities.[140,141] Existing transducer bandwidths, data-acquisition rates and reconstruction pipelines cannot keep pace, forcing manufacturers to choose between throughput loss, low resolution measurements, or sparse spot checks.[142,143] Innovations in the design of transducers, data collection electronics, inspection equipment, and computational algorithms are required to enable UT to be effectively implemented in-line at industrial manufacturing scales.

Detection sensitivity and decoupling of features is another challenge. First, in-plane spatial resolution for air-coupled arrays or roller probes is typically limited to ~100 μm, which is insufficient to resolve the micro-voids, foil-edge burrs and sub-laminate cracks that most often trigger scrap or latent safety hazards.[55,144] Many of those critical defects also exhibit only weak acoustic contrast, so they remain undetectable even when the system is tuned for maximum sensitivity.[145] Beam-focusing with phased array transducers may improve lateral resolution, but still may require large volumes of sample data to train effective defect detection algorithms. Furthermore, validating ultrasound's ability to detect defects it is suited for (dry spots, Li metal plating, separator tears, gas bubbles, etc.) remains difficult since these are not directly observable by other inspection modes.

Additionally, implementations of UT in cell plants must continually adapt and evolve as cell manufacturers and automotive OEMs adjust their strategies to optimize cost, performance, while improving vehicle safety.[146] Electrode manufacturing processes often transfer across form factors, however the wide range of cell sizes, shapes, and internal constructions across pouch, prismatic, and cylindrical formats presents a significant engineering challenge. These variations demand customized fixturing, tailored scanning strategies, and specialized approaches to signal processing and data analysis. For example, 4680 cylindrical cells are thicker than many prismatic cells, requiring different signal frequencies to maintain high signal quality and adequate penetration. These challenges are further compounded by the lack of standardized inspection protocols or quality benchmarks in battery manufacturing, particularly for newer techniques like ultrasound.

Finally, although UT hardware costs have fallen in recent years, the total cost of ownership including couplant management, probe wear and high-performance computing still exceeds that of mature alternatives such as beta-gauge mass-thickness sensors or high-speed machine vision, making plant managers reluctant to justify full-coverage deployment.[147,148] Consequently, today's industrial consensus frames UT as a valuable complementary tool for offline diagnostics or targeted inline audits rather than a universal, primary inspection modality. **Table 4** compares some conventional battery inspection techniques to UT.

Addressing the challenges presented requires close collaboration between battery and UT companies. Signal quality optimization is one of the top concerns for customers of battery ultrasound equipment. For implementation in a lab setting, it is possible to optimize purely for signal quality using liquid or gel

coupling. However, for implementation in high-throughput gigafactories, there must be a balance of throughput, complexity, and operational risk in determining the optimal solution. Dry coupling, which can achieve good signal quality with the use of specialized elastomers, strikes a balance by avoiding the complexity and risk associated with liquid and gel coupling.

Table 5. Comparison of conventional battery inspection techniques with UT

	Pros with respect to UT	**Cons with respect to UT**
X-ray / CT[149,150]	• True volumetric image of internal features • No contact/couplant • Mature defect libraries	• Ionizing radiation: shielding/licensing • Higher capital and operating expenses • Throughput limited for full CT (~mins-hours per cell)
Beta Gauges[105,116]	• Simple scalar output; easy PLC feedback • Excellent long-term stability (ppm drift) • Immune to surface gloss/color	• Radioisotope handling/disposal costs • Gives *average* thickness only—misses local voids/delaminations • Licensing paperwork per line/site
Visible Light Imaging[151,152]	• Sub-10 µm pixel resolution at >100 meters per minute • Lowest per-channel cost • Instantly interpretable images	• Cannot see beneath top surface • Sensitive to reflectivity & dust; needs custom lighting • High false-positive rate on cosmetic blemishes

In order to improve defect sensitivity and identification, it is important for UT companies and researchers to partner with manufacturers to build representative datasets by introducing controlled defects or process variations, which then inform predictive models. Quantity and quality of data is especially important when machine learning is leveraged to improve defect detection capabilities. A complementary strategy is to leverage physical simulation to accelerate system configuration and signal feature selection for specific detection applications. This approach can be used, for example, to guide defect detection by informing how

to set measurement parameters in the real world, as well as quickly determining where in the resulting measurement signal to look for meaningful features during analysis.

Looking ahead, the path to broader adoption of in-line ultrasound inspection can be accelerated with a phased approach: starting with in-line process monitoring to establish a robust data foundation, then layering on targeted defect detection and classification as models mature. To maximize the value of in-line inspection, manufacturing equipment and inspection systems need to be digitally connected. This connectivity enables detection of quality issues, traceability to the root cause or specific process steps, and monitoring of production performance and consistency. As ultrasound systems are deployed more widely and digitally connected quality control systems become more accepted, we anticipate the emergence of shared standards and stronger integration with complementary inspection methods, unlocking more predictive, data-driven process control across the battery manufacturing line.[153]

Perspectives and Future Applications

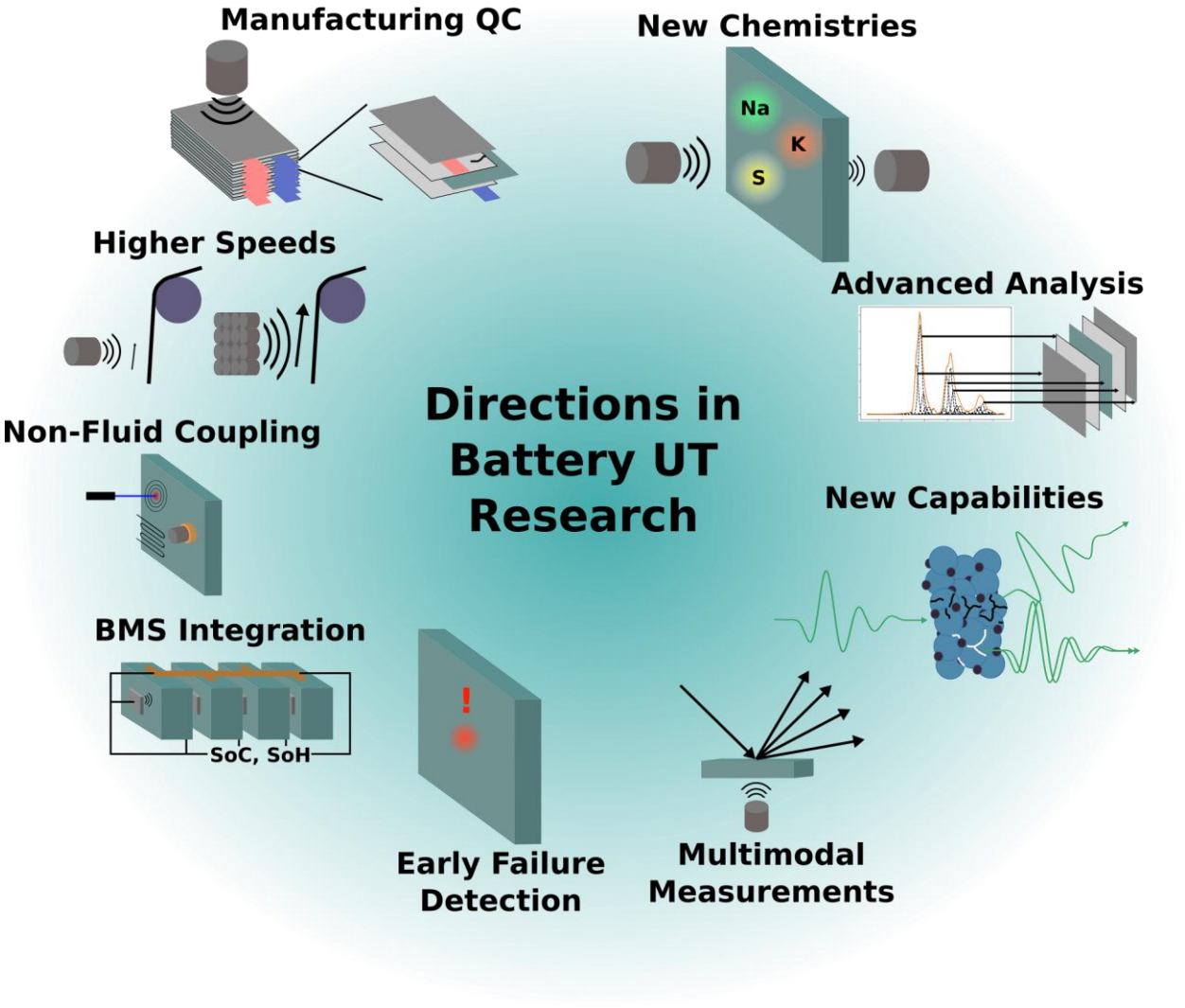

Figure 6. Summary of future directions in battery ultrasound research.

Ultrasound has been established as a fast, nondestructive technique for battery characterization and shows promise for inline quality control in manufacturing. Due to its accessibility, we expect routine use of UT in battery research to continue to grow as an easy complementary measure to standard electrochemical characterization. With this, researchers should target several functional areas to improve the value of the technique for the wider community (**Figure 6**).

To promote the widespread adoption of UT in battery literature and improve reproducibility, standardization of reporting is necessary. This standardization falls within two categories: physical setup and signal processing.

On the setup side, ultrasound hardware must be fully specified, including the pulse and measurement electronics, and the specific transducer models. The pulse shape should be included when possible, ideally through direct measurement in a simple system such as water or through a homogenous material such as steel or aluminum. Beyond listing the hardware, experimental details such as the transducer-battery distance (in a liquid- or air-coupled system), the couplant and clamping pressure (in a direct contact or solid-coupled system), and measurement temperature should be explicitly addressed. An explanation of how these parameters are kept constant, or exact measurements of their values, should be included.

Within the signal processing side, details of signal pre-processing such as hardware-level filters, oscilloscope downsampling, or post-collection digital processing must be specified, even when using default hardware values. Data processing and analysis code should also be accessible to researchers both to ensure reproducibility and help in widespread adoption of UT. All code should either use standard code libraries or be publicly available through free hosting platforms. Furthermore, user-specified parameters for data processing algorithms, such as those used in many ToF calculations, must be stated to ensure reproducibility of analysis.

Looking forward, UT studies should explore a wider array of relevant battery chemistries and formats. Future research should leverage UT to further study *operando* chemomechanical behaviors of next-generation electrodes and solid electrolytes. Furthermore, impact of cell formats past multilayer pouch cells warrants more rigorous analysis. Greater attention is needed for cylindrical and prismatic cells, particularly to understand acoustic propagation in cylindrical cans and enable more rigorous UT analysis of formats such as 18650 and 4680. Finally, the effect of cell constraint should be systematically examined. Existing studies employ a range of clamping approaches for pouch cells, despite the fact that constraint alters acoustic propagation and mechanical response. Additionally, cylindrical and prismatic cells have uniquely constrained configurations which could alter acoustic trends. Improved understanding of these factors can improve analysis and possibly inform setup standardization across the field.

Thus far, much UT battery research has studied SoC/SoH and failure tracking in a lab setting. To close the gap between research and field-deployed applications, studies should explore more realistic cycling protocols, considering the combined effects of faster C-rates, drive cycle conditions, and their consequent temperature effects. These behaviors must also be differentiated from those indicative of degradation and early-stage TR. Improved temperature compensation methods will likely be of increasing importance.

Even with these advancements on the research side, a significant challenge with implementing SoC/SoH tracking in field-deployed applications is the need for numerous, large datasets of UT data compared to SoC/SoH. Substantial amounts of data will be necessary for accurate predictions of single systems, and representative data will need to be collected for individual chemistries and formats. Optimized data collection and improved machine learning (ML) algorithms can support this. In addition to improvements in analysis, innovations in cheap UT hardware are needed to enable integration with a BMS. Low-cost CMUT arrays directly fabricated onto battery casings may be a route toward this goal, but other innovations may be possible.

There are several barriers to widespread industrial adoption of UT in battery manufacturing. While fluid-coupled transducers offer consistent contact and high signal, the need for immersion in a fluid makes them unsuitable for high-throughput manufacturing applications. Alternative coupling methods are needed that can match the signal offered by fluids. Air-coupled transducers, solid-coupled transducer arrays, EMATs or laser transducers are all promising candidates. Improvements in speed and spatial resolution are also desired for inline applications. Integrating cutting-edge transducer arrays into R&D efforts are needed to push these limits. Advances in medical imaging may also inspire this area. Using more advanced analysis, particularly data intensive ML-based ones, may also create computational bottlenecks. Algorithmic efficiency and the possibility of hardware-level processing are essential considerations for any inline technique.

Battery manufacturers have several measurement needs that could be met by ultrasound. Very few methods are available for identifying buried defects during the assembly phase. UT may be able to assist in this, but only if the above issues with coupling, resolutions, and speed are solved. Evaluation of the fragile tab welds is another area where ultrasound may be helpful, if improvements to depth resolution can be realized. Earlier in the manufacturing process, ultrasound could be used to complement viscosity, density, and particle size measurements. Following the coating process, UT is well suited for monitoring the drying and calendering process and identifying defects, provided measurement and analysis can be sped up to match the high speeds needed to run GWh-scale production facilities.

UT may also be used in second-life battery applications. As battery recycling becomes increasingly essential, companies seek to repurpose battery components, or in some cases, entire batteries.[154] The ability of UT to rapidly and nondestructively determine SoC and SoH suggests it will be a valuable tool for determining the suitability of a battery for recycling or second-life applications.

Any advancement in UT analysis should be accompanied by other measurement techniques for verification. The small footprint and simple instrumentation of UT makes it ideal for integration with other measurements, and multimodal experiments are an important part of the future of battery research. Beyond model verification or the scientists' urge to simply gather as much data as possible, future work should consider how simultaneous measurements can be leveraged to provide more information than would be possible with single measurements. An ultrasonic signal results from the complex interplay of mechanics and chemistry in a multilayered structure, and the more details that can be established by another measure, the more informative the ultrasound becomes.

Outside of specific research questions or industry needs, there are broad improvements to the UT technique that would be widely useful. Improvements in spatial resolution are needed. Wider adoption of focused transducers, laser methods, or improved image processing may be a path forward. Techniques from super-resolution microscopy that have been adapted by medical ultrasound researchers may be another source of inspiration.[155] The potential for high time resolution ultrasonic measurements has also been minimally explored in batteries. Under good conditions, PRF limited measurements can be performed on the 100 μs timescale. Investigating dynamic processes such as fast charging or TR may benefit from such high-speed measurements. Beyond improving resolution, there is a lot of information contained in an ultrasound measurement that is not well utilized. A fully deconvoluted pulse-echo measurement containing a back reflection theoretically carries information about every layer in a battery, meaning 3D tomography is in principle possible with SAM. In order to extract this information, advances in deconvolution and acoustic modeling are needed.

In addition, clever signal processing, use of multiple frequencies, or multimodal measurements may be ways to overcome the frequency - resolution - penetration depth tradeoff. Combining multiple measurements in different configurations or frequencies may also be used to reduce uncertainties or underdetermination in modeling of chemo-mechanical properties from acoustic data, as well as decouple

overlapping effects such as gassing and Li plating. To leverage these different techniques, a clearer understanding of UT rooted in fundamental acoustic physics rather than empirical correlations, is critical. This could help resolve some of the inconsistencies seen across different studies, particularly for SoH trends. More extensive acoustic modeling, informed by accurate material properties and layer-resolved models, could also enable new UT capabilities such as measurement of electrode porosity or monitoring crack formation. Finally, while studies on emerging chemistries often extend the same methods used on conventional systems, materials such as Li metal, sulfur, and solid electrolytes undergo fundamentally different mechanical evolution, motivating dedicated modeling and analysis for these systems.

Ultrasonic NDE is a well-established field, and techniques developed for e.g. geology or medical imaging may prove useful for batteries. We urge readers interested in developing battery UT to search the literature in journals outside of the battery field, as many problems we encounter now have likely been discussed in a different form decades ago. Readers who may be involved in ultrasound research in other domains - come over to the battery side. The problems are interesting and the results might shock you.

Acknowledgments

Declaration of Interests

Supplemental Information

Further details of signal processing methods, including signal amplitude, ToF, and damping.

References

1. Rajaeifar, M.A., Ghadimi, P., Raugei, M., Wu, Y., and Heidrich, O. (2022). Challenges and recent developments in supply and value chains of electric vehicle batteries: A sustainability perspective. Resour. Conserv. Recycl. *180*, 106144. https://doi.org/10.1016/j.resconrec.2021.106144.

2. Ensminger, D., and Bond, L.J. (2023). Ultrasonics: Fundamentals, technologies, and applications 4th Edition. (CRC Press) https://doi.org/10.1201/9780429286964.

3. Majasan, J.O., Robinson, J.B., Owen, R.E., Maier, M., Radhakrishnan, A.N.P., Pham, M., Tranter, T.G., Zhang, Y., Shearing, P.R., and Brett, D.J.L. (2021). Recent advances in acoustic diagnostics for electrochemical power systems. J. Phys. Energy *3*, 032011. https://doi.org/10.1088/2515-7655/abfb4a.

4. McGovern, M.E., Bruder, D.D., Huemiller, E.D., Rinker, T.J., Bracey, J.T., Sekol, R.C., and Abell, J.A. (2023). A review of research needs in nondestructive evaluation for quality verification in electric vehicle lithium-ion battery cell manufacturing. J. Power Sources *561*, 232742–232742. https://doi.org/10.1016/J.JPOWSOUR.2023.232742.

5. Deng, Z., Lin, X., Huang, Z., Meng, J., Zhong, Y., Ma, G., Zhou, Y., Shen, Y., Ding, H., and Huang, Y. (2021). Recent Progress on Advanced Imaging Techniques for Lithium-Ion Batteries. Adv. Energy Mater. *11*, 2000806–2000806. https://doi.org/10.1002/AENM.202000806.

6. Gold, L., Herzog, T., Schubert, F., Heuer, H., and Giffin, G.A. (2023). Ultrasound Propagation in Lithium-Ion Battery Cell Materials: Basis for Developing Monitoring and Imaging Methods. Energy Technol. *11*. https://doi.org/10.1002/ente.202200861.

7. Chang, W., Mohr, R., Kim, A., Raj, A., Davies, G., Denner, K., Park, J.H., and Steingart, D. (2020). Measuring effective stiffness of Li-ion batteries via acoustic signal processing. J. Mater. Chem. A Mater. Energy Sustain. *8*, 16624–16635. https://doi.org/10.1039/D0TA05552B.

8. Kinsler, L.E., Frey, A.R., Coppens, A.B., and Sanders, J.V. (1999). Fundamentals of Acoustics 4th ed. (John Wiley & Sons).

9. Briggs, A. (1992). Acoustic microscopy-a summary. Rep. Prog. Phys. *55*, 851–909. https://doi.org/10.1088/0034-4885/55/7/001.

10. Luijten, B., Chennakeshava, N., Eldar, Y.C., Mischi, M., and van Sloun, R.J.G. (2023). Ultrasound signal processing: From models to deep learning. Ultrasound Med. Biol. *49*, 677–698. https://doi.org/10.1016/j.ultrasmedbio.2022.11.003.

11. Knehr, K.W., Hodson, T., Bommier, C., Davies, G., Kim, A., and Steingart, D.A. (2018). Understanding full-cell evolution and non-chemical electrode crosstalk of Li-ion batteries. Joule *2*, 1146–1159. https://doi.org/10.1016/j.joule.2018.03.016.

12. Qi, Y., Hector, L.G., Jr, James, C., and Kim, K.J. (2014). Lithium concentration dependent elastic properties of battery electrode materials from first principles calculations. J. Electrochem. Soc. *161*, F3010–F3018. https://doi.org/10.1149/2.0031411jes.

13. Doh, C.-H., Han, B.-C., Jin, B.-S., and Gu, H.-B. (2011). Structures and Formation Energies of LixC6(x=1-3) and its Homologues for Lithium Rechargeable Batteries. Bull. Korean Chem. Soc. *32*, 2045–2050. https://doi.org/10.5012/bkcs.2011.32.6.2045.

14. Jie, G., Yifan, Z., Yan, L., Xiangling, W., Yang, L., Bin, W., and Cunfu, H. (2025). A novel ultrasonic transmission coefficient spectrums approach to detecting lithium deposition of lithium-ion batteries. J. Power Sources *636*, 236555. https://doi.org/10.1016/j.jpowsour.2025.236555.

15. Ladpli, P., Kopsaftopoulos, F., and Chang, F.-K. (2018). Estimating state of charge and health of lithium-ion batteries with guided waves using built-in piezoelectric sensors/actuators. J. Power Sources *384*, 342–354. https://doi.org/10.1016/j.jpowsour.2018.02.056.

16. Swallow, J.G., Woodford, W.H., McGrogan, F.P., Ferralis, N., Chiang, Y.-M., and Van Vliet, K.J. (2014). Effect of electrochemical charging on elastoplastic properties and fracture toughness of LiXCoO2. J. Electrochem. Soc. *161*, F3084–F3090. https://doi.org/10.1149/2.0141411jes.

17. Davies, G., Knehr, K.W., Van Tassell, B., Hodson, T., Biswas, S., Hsieh, A.G., and Steingart, D.A. (2017). State of Charge and State of Health Estimation Using Electrochemical Acoustic Time of Flight Analysis. J. Electrochem. Soc. *164*, A2746–A2755. https://doi.org/10.1149/2.1411712jes.

18. Ledbetter, H.M., and Naimon, E.R. (1974). Elastic properties of metals and alloys. II. Copper. J. Phys. Chem. Ref. Data *3*, 897–935. https://doi.org/10.1063/1.3253150.

19. ASM International (1990). ASM handbook vol. 2: Nonferrous alloys and special-purpose materials (ASM International).

20. Amsterdam, S., and Chang, W. (2025). Design of a low-cost ultrasonic testing instrument for battery

metrology. Electrochim. Acta *524*, 146012. https://doi.org/10.1016/j.electacta.2025.146012.

21. Wasylowski, D., Kisseler, N., Ditler, H., Sonnet, M., Fuchs, G., Ringbeck, F., and Sauer, D.U. (2022). Spatially resolving lithium-ion battery aging by open-hardware scanning acoustic imaging. J. Power Sources *521*, 230825–230825. https://doi.org/10.1016/J.JPOWSOUR.2021.230825.

22. Wasylowski, D., Neubauer, S., Faber, M., Ditler, H., Sonnet, M., Blömeke, A., Dechent, P., Gitis, A., and Sauer, D.U. (2023). In situ tomography of lithium-ion battery cells enabled by scanning acoustic imaging. J. Power Sources *580*, 233295–233295. https://doi.org/10.1016/j.jpowsour.2023.233295.

23. Feiler, S., Gold, L., Hartmann, S., and Giffin, G.A. (2024). Investigation of Acoustic Attenuation and Resonances in Lithium-Ion Batteries using Ultrasound Spectroscopy. Batter. Supercaps. https://doi.org/10.1002/BATT.202400212.

24. Xu, W., Li, L., Shi, F., and Chen, Q. (2025). Ultrasonic spectroscopy for in situ early detection and dynamic monitoring of lithium plating in lithium-ion batteries. Cell Rep. Phys. Sci. *6*, 102507. https://doi.org/10.1016/j.xcrp.2025.102507.

25. Shen, Y., Zou, B., Zhang, Z., Xu, M., Wang, S., Li, Q., Li, H., Zhou, M., Jiang, K., and Wang, K. (2023). In situ detection of lithium-ion batteries by ultrasonic technologies. Energy Storage Mater. *62*, 102915. https://doi.org/10.1016/j.ensm.2023.102915.

26. Wasylowski, D., Ditler, H., Sonnet, M., Falkenstein, T., Leogrande, L., Ronge, E., Blömeke, A., Würsig, A., Ringbeck, F., and Sauer, D.U. (2024). Operando visualisation of lithium plating by ultrasound imaging of battery cells. Nature Communications 2024 15:1 *15*, 1–11. https://doi.org/10.1038/s41467-024-54319-6.

27. Copley, R.J., Cumming, D., Wu, Y., and Dwyer-Joyce, R.S. (2021). Measurements and modelling of the response of an ultrasonic pulse to a lithium-ion battery as a precursor for state of charge estimation. J. Energy Storage *36*, 102406–102406. https://doi.org/10.1016/J.EST.2021.102406.

28. Gao, J., Lyu, Y., Chen, H., Song, W., Liu, H., Wu, B., and He, C. (2024). Guided waves propagation in lithium-ion batteries: Theoretical modeling and experimental analysis. NDT & E International *145*, 103102–103102. https://doi.org/10.1016/J.NDTEINT.2024.103102.

29. Mitra, M., and Gopalakrishnan, S. (2016). Guided wave based structural health monitoring: A review. Smart Mater. Struct. *25*, 053001. https://doi.org/10.1088/0964-1726/25/5/053001.

30. Schmerr, L.W. (1998). Fundamentals of Ultrasonic Nondestructive Evaluation (Springer US) https://doi.org/10.1007/978-1-4899-0142-2.

31. Xia, J., Wang, J., Yang, C., Wu, Y., Huang, P., and Lu, Y. (2025). Ultrasound-based battery state-of-charge monitoring and health evaluation using high directivity MEMS transducer. In 2025 23rd International Conference on Solid-State Sensors, Actuators and Microsystems (Transducers) (IEEE), pp. 1792–1795. https://doi.org/10.1109/transducers61432.2025.11109865.

32. Shung, K.K., and Zippuro, M. (1996). Ultrasonic transducers and arrays. IEEE Eng. Med. Biol. Mag. *15*, 20–30. https://doi.org/10.1109/51.544509.

33. Xu, W., Yang, Y., Shi, F., Li, L., Wen, F., and Chen, Q. (2023). Ultrasonic phased array imaging of gas evolution in a lithium-ion battery. Cell Rep. Phys. Sci. *4*, 101579.

https://doi.org/10.1016/j.xcrp.2023.101579.

34. Robinson, J.B., Owen, R.E., Kok, M.D.R., Maier, M., Majasan, J., Braglia, M., Stocker, R., Amietszajew, T., Roberts, A.J., Bhagat, R., et al. (2020). Identifying defects in Li-ion cells using ultrasound acoustic measurements. J. Electrochem. Soc. *167*, 120530. https://doi.org/10.1149/1945-7111/abb174.

35. Liu, X., Lyu, Y., Gao, J., Geng, M., Fan, M., Han, Z., and Zhang, C. (2025). Non-destructive estimation of internal state for lithium-ion batteries by ultrasonic phased array scanning and imaging technologies. J. Energy Storage *117*, 116155. https://doi.org/10.1016/j.est.2025.116155.

36. Zhou, Z., Hua, W., Peng, S., Tian, Y., Tian, J., and Li, X. (2024). Fast and smart state characterization of large-format lithium-ion batteries via phased-array ultrasonic sensing technology. Sensors (Basel) *24*, 7061. https://doi.org/10.3390/s24217061.

37. Shen, Y., Deng, Z., and Huang, Y. (2020). Ultrasonic scanning device and an application and method thereof. US Patent.

38. Shull, P.J., and Tittmann, B.R. (2002). Ultrasound. In Nondestructive Evaluation: Theory, Techniques, and Applications, P. J. Shull, ed. (CRC Press), pp. 63–192.

39. Mirkhani, K., Chaggares, C., Masterson, C., Jastrzebski, M., Dusatko, T., Sinclair, A., Shapoorabadi, R.J., Konrad, A., and Papini, M. (2004). Optimal design of EMAT transmitters. NDT E Int. *37*, 181–193. https://doi.org/10.1016/j.ndteint.2003.09.005.

40. Li, X., Yu, X., Tian, Y., Tian, J., and Xiong, R. (2024). Battery state characterization based on a contactless electromagnetic ultrasound testing method. J. Energy Storage *100*, 113499. https://doi.org/10.1016/j.est.2024.113499.

41. Chen, S.-L. (2016). Review of laser-generated ultrasound transmitters and their applications to all-optical ultrasound transducers and imaging. Appl. Sci. (Basel) *7*, 25. https://doi.org/10.3390/app7010025.

42. Tang, D., Xu, C., Xu, G., Cui, S., and Zhang, S. (2025). Non-contact laser ultrasound detection of internal gas defects in lithium-ion batteries. Sensors (Basel) *25*, 2033. https://doi.org/10.3390/s25072033.

43. Sampath, S., Yin, X., Tham, Z.W., Chen, Y.F., and Zhang, L. (2024). Real-time and non-contact estimation of state of charge for lithium-ion battery using laser ultrasonics. J. Power Sources *605*, 234544. https://doi.org/10.1016/j.jpowsour.2024.234544.

44. Zhou, D., Chen, F., Liang, J., Zhang, Y., Zheng, W., and Li, X. (2025). Battery defect detection using ultrasonic guided waves and a convolutional neural network model. J. Energy Storage *119*, 116352. https://doi.org/10.1016/j.est.2025.116352.

45. Brenner, K., Ergun, A.S., Firouzi, K., Rasmussen, M.F., Stedman, Q., and Khuri-Yakub, B.P. (2019). Advances in capacitive micromachined ultrasonic transducers. Micromachines (Basel) *10*, 152. https://doi.org/10.3390/mi10020152.

46. Joseph, J., Ma, B., and Khuri-Yakub, B.T. (2022). Applications of capacitive micromachined ultrasonic transducers: A comprehensive review. IEEE Trans. Ultrason. Ferroelectr. Freq. Control *69*, 456–467. https://doi.org/10.1109/TUFFC.2021.3112917.

47. Cannon, A. (2023). Li-ion cell in operando monitoring and prognostication using CMUT devices. Meet. Abstr. *MA2023-02*, 2926–2926. https://doi.org/10.1149/ma2023-02622926mtgabs.

48. Chen, J., Fei, C., Lin, D., Gao, P., Zhang, J., Quan, Y., Chen, D., Li, D., and Yang, Y. (2022). A review of UltraHigh frequency ultrasonic transducers. Front. Mater. *8*, 733358. https://doi.org/10.3389/fmats.2021.733358.

49. Kazys, R., and Vaskeliene, V. (2021). High temperature ultrasonic transducers: A review. Sensors (Basel) *21*, 3200. https://doi.org/10.3390/s21093200.

50. Ren, D., Yin, Y., Li, C., Chen, R., and Shi, J. (2023). Recent advances in flexible ultrasonic transducers: From materials optimization to imaging applications. Micromachines (Basel) *14*, 126. https://doi.org/10.3390/mi14010126.

51. Krautkrämer, J., and Krautkrämer, H. (1990). Ultrasonic testing of materials 4th ed. (Springer) https://doi.org/10.1007/978-3-662-10680-8.

52. Meng, K., Chen, X., Zhang, W., Chang, W., and Xu, J. (2022). A robust ultrasonic characterization methodology for lithium-ion batteries on frequency-domain damping analysis. J. Power Sources *547*, 232003. https://doi.org/10.1016/j.jpowsour.2022.232003.

53. Sun, K., Thorsteinsson, G., Stiber, A., Katzman, L., Chang, W., May, R., and Steingart, D.A. (2024). Chemo-mechanical hysteresis of sulfur conversion electrodes via operando acoustic transmission. J. Electrochem. Soc. *171*, 100504. https://doi.org/10.1149/1945-7111/ad803b.

54. Huang, M., Kirkaldy, N., Zhao, Y., Patel, Y., Cegla, F., and Lan, B. (2022). Quantitative characterisation of the layered structure within lithium-ion batteries using ultrasonic resonance. J. Energy Storage *50*, 104585–104585. https://doi.org/10.1016/J.EST.2022.104585.

55. Bauermann, L.P., Mesquita, L.V., Bischoff, C., Drews, M., Fitz, O., Heuer, A., and Biro, D. (2020). Scanning acoustic microscopy as a non-destructive imaging tool to localize defects inside battery cells. Journal of Power Sources Advances *6*, 100035. https://doi.org/10.1016/j.powera.2020.100035.

56. Vaezi, Y., and Van der Baan, M. (2015). Comparison of the STA/LTA and power spectral density methods for microseismic event detection. Geophys. J. Int. *203*, 1896–1908. https://doi.org/10.1093/gji/ggv419.

57. Cai, Z., Pan, T., Jiang, H., Li, Z., and Wang, Y. (2023). State-of-charge estimation of lithium-ion batteries based on ultrasonic detection. J. Energy Storage *65*, 107264. https://doi.org/10.1016/j.est.2023.107264.

58. Hodson, T., Patil, S., and Steingart, D.A. (2021). An initial exploration of coupled transient mechanical and electrochemical behaviors in lithium ion batteries. J. Electrochem. Soc. *168*, 070515. https://doi.org/10.1149/1945-7111/ac0f86.

59. Liu, X., Deng, Z., Liao, Y., Du, J., Tian, J., Liu, Z., Shen, Y., and Huang, Y. (2023). Decoupling of the anode and cathode ultrasonic responses to the state of charge of a lithium-ion battery. Phys. Chem. Chem. Phys. *25*, 21730–21735. https://doi.org/10.1039/d2cp05948g.

60. Robinson, J.B., Pham, M., Kok, M.D.R., Heenan, T.M.M., Brett, D.J.L., and Shearing, P.R. (2019). Examining the cycling behaviour of Li-ion batteries using ultrasonic time-of-flight measurements. J. Power Sources *444*, 227318. https://doi.org/10.1016/j.jpowsour.2019.227318.

61. Renais, C., Mercier-Guyon, B., Wasylowski, D., Sonnet, M., Dechent, P., Servajon, M., Blanc, N., Lyonnard, S., Sauer, D.U., and Villevieille, C. (2025). Exploring electrochemical dynamics in graphite||LiNiMnCoO cells via operando ultrasound and multiprobe approaches. Nat Commun *16*, 7774. https://doi.org/10.1038/s41467-025-62935-z.

62. Hsieh, A.G., Bhadra, S., Hertzberg, B.J., Gjeltema, P.J., Goy, A., Fleischer, J.W., and Steingart, D.A. (2015). Electrochemical-acoustic time of flight: in operando correlation of physical dynamics with battery charge and health. Energy Environ. Sci. *8*, 1569–1577. https://doi.org/10.1039/C5EE00111K.

63. Qi, Y., Guo, H., Hector, L.G., and Timmons, A. (2010). Threefold increase in the young's modulus of graphite negative electrode during lithium intercalation. J. Electrochem. Soc. *157*, A558. https://doi.org/10.1149/1.3327913.

64. C P, S., Bibin, J., and C, G. (2014). Lithium titanate as anode material for lithium-ion cells: a review. Ionics (Kiel) *20*, 601–620. https://doi.org/10.1007/s11581-014-1113-4.

65. Hertzberg, B., Benson, J., and Yushin, G. (2011). Ex-situ depth-sensing indentation measurements of electrochemically produced Si–Li alloy films. Electrochem. Commun. *13*, 818–821. https://doi.org/10.1016/j.elecom.2011.05.011.

66. Berla, L.A., Lee, S.W., Cui, Y., and Nix, W.D. (2015). Mechanical behavior of electrochemically lithiated silicon. J. Power Sources *273*, 41–51. https://doi.org/10.1016/j.jpowsour.2014.09.073.

67. Feyzi, E., Kumar, A., Li, X., Deng, S., Nanda, J., and Zaghib, K. (2024). A comprehensive review of silicon anodes for high-energy lithium-ion batteries: Challenges, latest developments, and perspectives. Next Energy *5*, 100176. https://doi.org/10.1016/j.nxener.2024.100176.

68. Stallard, J.C., Wheatcroft, L., Booth, S.G., Boston, R., Corr, S.A., De Volder, M.F.L., Inkson, B.J., and Fleck, N.A. (2022). Mechanical properties of cathode materials for lithium-ion batteries. Joule *6*, 984–1007. https://doi.org/10.1016/j.joule.2022.04.001.

69. Ihlbrock, L., Sehnal, A., Gutsch, M., and Lux, S. (2025). Future energy demand for automotive and stationary lithium- and sodium-ion battery production towards a European circular economy. Energy Environ. Sci. *18*, 8724–8743. https://doi.org/10.1039/d5ee02287h.

70. Yi, T.-F., Xie, Y., Zhu, Y.-R., Shu, J., Zhou, A.-N., and Qiao, H.-B. (2012). Stabilities and electronic properties of lithium titanium oxide anode material for lithium ion battery. J. Power Sources *198*, 318–321. https://doi.org/10.1016/j.jpowsour.2011.10.014.

71. Jain, A., Ong, S.P., Hautier, G., Chen, W., Richards, W.D., Dacek, S., Cholia, S., Gunter, D., Skinner, D., Ceder, G., et al. (2013). Commentary: The Materials Project: A materials genome approach to accelerating materials innovation. APL Mater. *1*, 011002. https://doi.org/10.1063/1.4812323.

72. de Jong, M., Chen, W., Angsten, T., Jain, A., Notestine, R., Gamst, A., Sluiter, M., Krishna Ande, C., van der Zwaag, S., Plata, J.J., et al. (2015). Charting the complete elastic properties of inorganic crystalline compounds. Sci. Data *2*, 150009. https://doi.org/10.1038/sdata.2015.9.

73. Maxisch, T., and Ceder, G. (2006). Elastic properties of olivine LixFePO4 from first principles. Phys. Rev. B Condens. Matter Mater. Phys. *73*, 174112. https://doi.org/10.1103/physrevb.73.174112.

74. Chang, W., Thorsteinsson, G., Janakiraman, U., Chowdhury, R.R., Herman, Z., Katzman, L., and Steingart, D.A. (2024). Relating Chemo-Mechanical Hysteresis and Formation Protocols for Anode-Free Lithium Metal Batteries. J. Electrochem. Soc. *171*, 040506. https://doi.org/10.1149/1945-7111/ad36e3.

75. Ponnekanti, A., Thorsteinsson, G., Wasylowski, D., Sun, K., May, R., Schumacher, B., Schwartz, B., Herman, Z., Katzman, L., Olushina, T., et al. (2025). *Operando* acoustic analysis of formation parameter coupling in lithium metal batteries. J. Electrochem. Soc. *172*, 030524. https://doi.org/10.1149/1945-7111/adc15a.

76. Sun, K., Thorsteinsson, G., Zhao, D., Owen, C., Ponnekanti, A., Herman, Z., Parris, B., Kothari, I., and Steingart, D.A. (2025). Chemo-mechanics and morphological dynamics of Si electrodes in all-solid-state Li-ion batteries. ACS Energy Lett. *10*, 1229–1234. https://doi.org/10.1021/acsenergylett.5c00132.

77. Bommier, C., Chang, W., Li, J., Biswas, S., Davies, G., Nanda, J., and Steingart, D. (2020). Operando Acoustic Monitoring of SEI Formation and Long-Term Cycling in NMC/SiGr Composite Pouch Cells. J. Electrochem. Soc. *167*, 020517. https://doi.org/10.1149/1945-7111/ab68d6.

78. Zhao, G., Liu, Y., Liu, G., Jiang, S., and Hao, W. (2021). State-of-charge and state-of-health estimation for lithium-ion battery using the direct wave signals of guided wave. J. Energy Storage *39*, 102657. https://doi.org/10.1016/j.est.2021.102657.

79. Wu, Y., Wang, Y., Yung, W.K.C., and Pecht, M. (2019). Ultrasonic health monitoring of lithium-ion batteries. Electronics (Basel) *8*, 751. https://doi.org/10.3390/electronics8070751.

80. Kim, J.-Y., Jo, J.-H., and Byeon, J.-W. (2020). Ultrasonic monitoring performance degradation of lithium ion battery. Microelectron. Reliab. *114*, 113859. https://doi.org/10.1016/j.microrel.2020.113859.

81. Owen, R.E., Robinson, J.B., Weaving, J., Pham, M., Tranter, T.G., Neville, T.P., Billson, D., Braglia, M., Stocker, R., Ahlberg Tiblad, A., et al. (2022). Operando ultrasonic monitoring of lithium-ion battery temperature and behaviour at different cycling rates and under drive cycle conditions. J. Electrochem. Soc. *169*, 040563. https://doi.org/10.1149/1945-7111/ac6833.

82. Nguyen, T.D., Sun, H., Amin, R., Ramuhalli, P., Kweon, C.-B.M., and Belharouak, I. (2024). Ultrasonic nondestructive diagnosis of cylindrical batteries under various charging rates. J. Electrochem. Soc. *171*, 020522. https://doi.org/10.1149/1945-7111/ad2642.

83. Montoya-Bedoya, S., Garcia-Tamayo, E., Rohrbach, D., Gaviria-Cardona, J.P., Martinez-Tejada, H.V., Planden, B., Howey, D.A., Florez, W.F., Valencia, R.A., and Bernal, M. (2024). Quantitative ultrasound spectroscopy for screening cylindrical lithium-ion batteries for second-life applications. Batter. Supercaps *7*, e202400002. https://doi.org/10.1002/batt.202400002.

84. Kirchev, A., Guillet, N., Brun-Buission, D., and Gau, V. (2022). Li-ion cell safety monitoring using mechanical parameters: Part I. normal battery operation. J. Electrochem. Soc. *169*, 010515. https://doi.org/10.1149/1945-7111/ac48c8.

85. Salso, P., Genovés, V., Merillas Valero, B., and Gómez Álvarez-Arenas, T. (2025). Testing of polymeric battery separators using air-coupled, high-frequency and wideband ultrasonic pulses. Polym. Test. *148*, 108837. https://doi.org/10.1016/j.polymertesting.2025.108837.

86. Gold, L., Bach, T., Virsik, W., Schmitt, A., Müller, J., Staab, T.E.M., and Sextl, G. (2017). Probing lithium-ion batteries' state-of-charge using ultrasonic transmission – Concept and laboratory testing. J. Power Sources *343*, 536–544. https://doi.org/10.1016/j.jpowsour.2017.01.090.

87. Popp, H., Koller, M., Keller, S., Glanz, G., Klambauer, R., and Bergmann, A. (2019). State estimation approach of lithium-ion batteries by simplified ultrasonic time-of-flight measurement. IEEE Access *7*, 170992–171000. https://doi.org/10.1109/access.2019.2955556.

88. Pham, M.T.M., Darst, J.J., Finegan, D.P., Robinson, J.B., Heenan, T.M.M., Kok, M.D.R., Iacoviello, F., Owen, R., Walker, W.Q., Magdysyuk, O.V., et al. (2020). Correlative acoustic time-of-flight spectroscopy and X-ray imaging to investigate gas-induced delamination in lithium-ion pouch cells during thermal runaway. J. Power Sources *470*, 228039. https://doi.org/10.1016/j.jpowsour.2020.228039.

89. Owen, R.E., Wiśniewska, E., Braglia, M., Stocker, R., Shearing, P.R., Brett, D.J.L., and Robinson, J.B. (2024). Operando Ultrasonic Monitoring of the Internal Temperature of Lithium-ion Batteries for the Detection and Prevention of Thermal Runaway. J. Electrochem. Soc. *171*, 040525. https://doi.org/10.1149/1945-7111/ad3beb.

90. Deng, Z., Huang, Z., Shen, Y., Huang, Y., Ding, H., Luscombe, A., Johnson, M., Harlow, J.E., Gauthier, R., and Dahn, J.R. (2020). Ultrasonic Scanning to Observe Wetting and "Unwetting" in Li-Ion Pouch Cells. Joule *4*, 2017–2029. https://doi.org/10.1016/j.joule.2020.07.014.

91. Kaden, N., Schlimbach, R., Rohde García, Á., and Dröder, K. (2023). A Systematic Literature Analysis on Electrolyte Filling and Wetting in Lithium-Ion Battery Production. Batteries *9*, 1–22. https://doi.org/10.3390/batteries9030164.

92. Louli, A.J., Eldesoky, A., Weber, R., Genovese, M., Coon, M., deGooyer, J., Deng, Z., White, R.T., Lee, J., Rodgers, T., et al. (2020). Diagnosing and correcting anode-free cell failure via electrolyte and morphological analysis. Nature Energy *5*, 693–702. https://doi.org/10.1038/s41560-020-0668-8.

93. Huo, H., Huang, K., Luo, W., Meng, J., Zhou, L., Deng, Z., Wen, J., Dai, Y., Huang, Z., Shen, Y., et al. (2022). Evaluating interfacial stability in solid-state pouch cells via ultrasonic imaging. ACS Energy Lett. *7*, 650–658. https://doi.org/10.1021/acsenergylett.1c02363.

94. Pei, F., Wu, L., Zhang, Y., Liao, Y., Kang, Q., Han, Y., Zhang, H., Shen, Y., Xu, H., Li, Z., et al. (2024). Interfacial self-healing polymer electrolytes for long-cycle solid-state lithium-sulfur batteries. Nat. Commun. *15*, 351. https://doi.org/10.1038/s41467-023-43467-w.

95. Chang, W., and Steingart, D. (2021). Operando 2D Acoustic Characterization of Lithium-Ion Battery Spatial Dynamics. ACS Energy Lett. *6*, 2960–2968. https://doi.org/10.1021/acsenergylett.1c01324.

96. Bommier, C., Chang, W., Lu, Y., Yeung, J., Davies, G., Mohr, R., Williams, M., and Steingart, D. (2020). In operando acoustic detection of lithium metal plating in commercial LiCoO2/graphite pouch cells. Cell Rep. Phys. Sci. *1*, 100035. https://doi.org/10.1016/j.xcrp.2020.100035.

97. Meyer, J., Dietz, A., Zhan, M., Fill, A., and Birke, K.P. (2025). Spatially resolved, in operando detection of reversible lithium plating using ultrasonic waves. J. Power Sources *653*, 237723. https://doi.org/10.1016/j.jpowsour.2025.237723.

98. McGee, T.M., Neath, B., Matthews, S., Ezekoye, O.A., and Haberman, M.R. (2023). Ultrasonic inspection of lithium-ion pouch cells subjected to localized thermal abuse. J. Power Sources *583*,

233542. https://doi.org/10.1016/j.jpowsour.2023.233542.

99. Zhang, L., Wei, Z., Liu, C., He, H., Liu, K., Zhou, G., Huang, Y., and Xu, Z.J. (2025). One ultrasonic measurement for non-invasive and whole-life-cycle thermal diagnosis of lithium-ion batteries. Energy Environ. Sci. *18*, 7894–7904. https://doi.org/10.1039/d5ee01892g.

100. Chang, W., Bommier, C., Fair, T., Yeung, J., Patil, S., and Steingart, D. (2020). Understanding adverse effects of temperature shifts on Li-ion batteries: An operando acoustic study. J. Electrochem. Soc. *167*, 090503. https://doi.org/10.1149/1945-7111/ab6c56.

101. Appleberry, M.C., Kowalski, J.A., Africk, S.A., Mitchell, J., Ferree, T.C., Chang, V., Parekh, V., Xu, Z., Ye, Z., Whitacre, J.F., et al. (2022). Avoiding thermal runaway in lithium-ion batteries using ultrasound detection of early failure mechanisms. J. Power Sources *535*, 231423. https://doi.org/10.1016/j.jpowsour.2022.231423.

102. Liu, D., Shadike, Z., Lin, R., Qian, K., Li, H., Li, K., Wang, S., Yu, Q., Liu, M., Ganapathy, S., et al. (2019). Review of Recent Development of In Situ/Operando Characterization Techniques for Lithium Battery Research. Adv. Mater. *31*, 1806620–1806620. https://doi.org/10.1002/ADMA.201806620.

103. Grant, A., and O'dwyer, C. (2023). Real-time nondestructive methods for examining battery electrode materials. Appl. Phys. Rev. *10*. https://doi.org/10.1063/5.0107386/2881289.

104. Shen, Y., Wang, S., Li, H., Wang, K., and Jiang, K. (2023). An overview on in situ/operando battery sensing methodology through thermal and stress measurements. J. Energy Storage *64*, 107164–107164. https://doi.org/10.1016/J.EST.2023.107164.

105. Gervillié-Mouravieff, C., Bao, W., Steingart, D.A., and Meng, Y.S. (2024). Non-destructive characterization techniques for battery performance and life-cycle assessment. Nature Reviews Electrical Engineering 2024 1:8 *1*, 547–558. https://doi.org/10.1038/s44287-024-00069-y.

106. Zuo, W., Liu, R., Cai, J., Hu, Y., Almazrouei, M., Liu, X., Cui, T., Jia, X., Apodaca, E., Alami, J., et al. (2025). Nondestructive analysis of commercial batteries. Chem. Rev. *125*, 369–444. https://doi.org/10.1021/acs.chemrev.4c00566.

107. Tan, J., Liu, D., Xu, X., and Mai, L. (2017). In situ/operando characterization techniques for rechargeable lithium-sulfur batteries: a review. Nanoscale *9*, 19001–19016. https://doi.org/10.1039/c7nr06819k.

108. Zappen, H., Fuchs, G., Gitis, A., and Sauer, D. (2020). In-operando impedance spectroscopy and ultrasonic measurements during high-temperature abuse experiments on lithium-ion batteries. Batteries *6*, 25. https://doi.org/10.3390/batteries6020025.

109. Robinson, J.B., Maier, M., Alster, G., Compton, T., Brett, D.J.L., and Shearing, P.R. (2019). Spatially resolved ultrasound diagnostics of Li-ion battery electrodes. Phys. Chem. Chem. Phys. *21*, 6354–6361. https://doi.org/10.1039/c8cp07098a.

110. Chang, W., May, R., Wang, M., Thorsteinsson, G., Sakamoto, J., Marbella, L., and Steingart, D. (2021). Evolving contact mechanics and microstructure formation dynamics of the lithium metal-Li7La3Zr2O12 interface. Nat. Commun. *12*, 6369. https://doi.org/10.1038/s41467-021-26632-x.

111. Fordham, A., Owen, R.E., Shearing, P.R., Robinson, J.B., and Jervis, R. (2025). Listening to

batteries: Using acoustic diagnostic techniques for electrochemical characterisation to improve battery performance and safety. Meet. Abstr. *MA2025-01*, 560–560. https://doi.org/10.1149/ma2025-015560mtgabs.

112. Fordham, A., Milojevic, Z., Giles, E., Du, W., Owen, R.E., Michalik, S., Chater, P.A., Das, P.K., Attidekou, P.S., Lambert, S.M., et al. (2023). Correlative non-destructive techniques to investigate aging and orientation effects in automotive Li-ion pouch cells. Joule *7*, 2622–2652.

113. Lee, H., Seo, Y.-H., and Ma, P.-S. (2025). Advanced ultrasonic detection of lithium-ion battery thermal runaway under various heating powers. Appl. Energy *396*, 126328. https://doi.org/10.1016/j.apenergy.2025.126328.

114. Sedláčková, E., Pražanová, A., Plachý, Z., Klusoňová, N., Knap, V., and Dušek, K. (2025). Acoustic emission technique for battery health monitoring: Comprehensive literature review. Batteries *11*, 14. https://doi.org/10.3390/batteries11010014.

115. Espinoza Ramos, I., Coric, A., Su, B., Zhao, Q., Eriksson, L., Krysander, M., Ahlberg Tidblad, A., and Zhang, L. (2024). Online acoustic emission sensing of rechargeable batteries: technology, status, and prospects. J. Mater. Chem. A Mater. Energy Sustain. *12*, 23280–23296. https://doi.org/10.1039/d4ta04571h.

116. Haghi, S., Leeb, M., Molzberger, A., and Daub, R. (2023). Measuring instruments for characterization of intermediate products in electrode manufacturing of lithium-ion batteries. Energy Technol. *11*. https://doi.org/10.1002/ente.202300364.

117. Reynolds, C.D., Slater, P.R., Hare, S.D., Simmons, M.J.H., and Kendrick, E. (2021). A review of metrology in lithium-ion electrode coating processes. Mater. Des. *209*, 109971. https://doi.org/10.1016/j.matdes.2021.109971.

118. Yang, Y., Guo, Z., Zhao, Y., Dong, H., Titirici, M.-M., Cegla, F., Pinfield, V., and Lan, B. (2026). Towards inline ultrasonic characterisation of battery slurry mixing: opportunities, challenges, and perspectives. Energy Environ. Sci. https://doi.org/10.1039/d5ee03563e.

119. Povey, M.J.W. (2013). Ultrasound particle sizing: A review. Particuology *11*, 135–147. https://doi.org/10.1016/j.partic.2012.05.010.

120. Bamberger, J.A., and Greenwood, M.S. (2004). Measuring fluid and slurry density and solids concentration non-invasively. Ultrasonics *42*, 563–567. https://doi.org/10.1016/j.ultras.2004.01.032.

121. Bamberger, J.A., and Greenwood, M.S. (2004). Using ultrasonic attenuation to monitor slurry mixing in real time. Ultrasonics *42*, 145–148. https://doi.org/10.1016/j.ultras.2004.02.016.

122. Zarrinkhat, F., Tadayand, P.F., and Arnone, D.D. (2023). Application of terahertz pulses to non-destructive testing. JNDE *20*, 35–43.

123. Bammer, F., and Huemer, F. (2019). Inline thickness measurement with imaging ellipsometry. In Photonics and Education in Measurement Science 2019, B. Zagar, P. Mazurek, M. Rosenberger, and P.-G. Dittrich, eds. (SPIE), pp. 98–101. https://doi.org/10.1117/12.2531940.

124. Cazorla Soult, M., Siller, V., Zhu, X., Gehlhaar, R., Wojcik, P.J., Morata, A., Tarancón, A., Vereecken, P.M., and Hubin, A. (2022). Spectroscopic ellipsometry for operando monitoring of (DE)lithiation-induced phenomena on $LiMn_2O_4$ and $LiNi_{0.5}Mn_{1.5}O_4$ electrodes. J. Electrochem. Soc.

169, 040501. https://doi.org/10.1149/1945-7111/ac5ceb.

125. Zhang, Y.S., Pallipurath Radhakrishnan, A.N., Robinson, J.B., Owen, R.E., Tranter, T.G., Kendrick, E., Shearing, P.R., and Brett, D.J.L. (2021). In situ ultrasound acoustic measurement of the lithium-ion battery electrode drying process. ACS Appl. Mater. Interfaces *13*, 36605–36620. https://doi.org/10.1021/acsami.1c10472.

126. Guk, E., Niri, M.F., Vincent, T.A., Apachitei, G., Briggs, C., Gulsoy, B., Chao, S., Guo, Z., Sansom, J.E.H., and Marco, J. (2024). Investigation of calendaring parameters on the microstructure of graphite anodes within lithium-ion batteries: Insights from ultrasonic testing. J. Power Sources *614*, 235063. https://doi.org/10.1016/j.jpowsour.2024.235063.

127. Tayamen, A.M.R., Amsterdam, S., and Chang, W.K. (2025). Air-coupled ultrasound for nondestructive evaluation of battery electrodes. ACS Energy Lett. https://doi.org/10.1021/acsenergylett.5c02422.

128. Attia, P.M., Moch, E., and Herring, P.K. (2025). Challenges and opportunities for high-quality battery production at scale. Nat. Commun. *16*, 611. https://doi.org/10.1038/s41467-025-55861-7.

129. Ilott, A.J., Mohammadi, M., Schauerman, C.M., Ganter, M.J., and Jerschow, A. (2018). Rechargeable lithium-ion cell state of charge and defect detection by in-situ inside-out magnetic resonance imaging. Nat. Commun. *9*, 1776. https://doi.org/10.1038/s41467-018-04192-x.

130. Copley, R.J., and Dwyer-Joyce, R.S. (2023). Prediction of the internal structure of a lithium-ion battery using a single ultrasound wave response. J. Energy Storage *72*, 108778–108778. https://doi.org/10.1016/J.EST.2023.108778.

131. McGovern, M.E., Bruder, D.D., James, R., and Gattani, V. (2022). Total Focusing Method with laser-generated ultrasonic waves for defect detection in finite plates. In ASNT 30th Research Symposium Conference Proceedings (The American Society for Nondestructive Testing Inc.), pp. 1–4. https://doi.org/10.32548/rs.2022.024.

132. Bruder, D.D., McGovern, M.E., James, R., Rinker, T.J., and Gattani, V. (2023). Assessment of laser-generated ultrasonic total focusing method for battery cell foil weld inspection. Res. Nondestruct. Eval., 1–18. https://doi.org/10.1080/09349847.2023.2195369.

133. Hwang, Y.-I., Park, J., Munir, N., Kim, H.-J., Song, S.-J., and Kim, K.-B. (2022). Discrimination of poor electrode junctions within lithium-ion batteries by ultrasonic measurement and deep learning. Batteries *8*, 21. https://doi.org/10.3390/batteries8030021.

134. Shan, D.O.U., Hsieh, A.G., Biswas, S., Van Tassell, B.J., Lee, E.M., Yu, D., and Yu, J.Y. (2023). Systems and methods for evaluating electrolyte wetting and distribution. US Patent.

135. Sun, B., Zhang, C., Liu, S., Xu, Z., and Li, L. (2024). Ultrasonic inspection of pouch-type lithium-ion batteries: a review. Nondestruct. Test. Eval., 1–34. https://doi.org/10.1080/10589759.2024.2317866.

136. Warren OH Location Ultium Cells LLC. https://www.ultiumcell.com/our-locations/warren-oh.

137. Holderith, P. (2024). Here’s An Exceedingly Nerdy Explanation of GM's Ultium Battery System. Motor1.com. https://www.motor1.com/features/717675/gm-ultium-battery-deep-dive/.

138. Compact Tape Casting Coater w/ Vac. Chuck (200Wx365L mm) & Film Applic MTI Online Store.

https://mtixtl.com/products/msk-afa-iii.

139. MSE PRO Automatic Film Coater For Battery Electrode Coating MSE Supplies LLC. https://www.msesupplies.com/products/mse-pro-automatic-film-coater-for-battery-electrode-coating.

140. Electrode Coating Solutions Durr Corporation. https://www.durr.com/fileadmin/durr.com/01_Products/14_Electromobility_battery/Energy_Storage/Electrode_Coating/duerr-megtec-li-ion-battery-electrode-manufacturing-en.pdf.

141. Pilot Line 1 University of Michigan Battery Lab. https://umbatterylab.engin.umich.edu/pilot-line-1/.

142. Lechner, M., Kollenda, A., Bendzuck, K., Burmeister, J.K., Mahin, K., Keilhofer, J., Kemmer, L., Blaschke, M.J., Friedl, G., Daub, R., et al. (2024). Cost modeling for the GWh-scale production of modern lithium-ion battery cells. Commun Eng *3*, 155. https://doi.org/10.1038/s44172-024-00306-0.

143. Maize, K., Mi, Y., Cakmak, M., and Shakouri, A. (2023). Real-time metrology for roll-to-roll and advanced inline manufacturing: A review. Adv. Mater. Technol. *8*, 2200173. https://doi.org/10.1002/admt.202200173.

144. Webster, M.R., Frankforter, E.L., and Juarez, P. (2023). Evaluation of ultrasonic battery inspection techniques. In Nondestructive Characterization and Monitoring of Advanced Materials, Aerospace, Civil Infrastructure, and Transportation XVII, P. J. Shull, T. Yu, A. L. Gyekenyesi, and H. F. Wu, eds. (SPIE), p. 28. https://doi.org/10.1117/12.2656667.

145. Chacón, X.C.A., Laureti, S., Ricci, M., and Cappuccino, G. (2023). A review of non-destructive techniques for lithium-ion battery performance analysis. World Electric Veh. J. *14*, 305. https://doi.org/10.3390/wevj14110305.

146. Link, S., Neef, C., and Wicke, T. (2023). Trends in automotive battery cell design: A statistical analysis of empirical data. Batteries *9*, 261. https://doi.org/10.3390/batteries9050261.

147. Soral, P. (2025). Machine Vision Systems: From Industry Applications to Cost Implications. Photoneo Focused on 3D. https://www.photoneo.com/machine-vision-systems-industry-applications-cost-implications/.

148. QA solutions for Battery Manufacturing TitanAES. https://www.titanaes.com/battery-manufacturing.

149. Wood, V. (2018). X-ray tomography for battery research and development. Nat. Rev. Mater. *3*, 293–295. https://doi.org/10.1038/s41578-018-0053-4.

150. Pietsch, P., and Wood, V. (2017). X-ray tomography for lithium ion battery research: A practical guide. Annu. Rev. Mater. Res. *47*, 451–479. https://doi.org/10.1146/annurev-matsci-070616-123957.

151. Huber, J., Tammer, C., Krotil, S., Waidmann, S., Hao, X., Seidel, C., and Reinhart, G. (2016). Method for classification of battery separator defects using optical inspection. Procedia CIRP *57*, 585–590. https://doi.org/10.1016/j.procir.2016.11.101.

152. Saariluoma, H., Piiroinen, A., Unt, A., Hakanen, J., Rautava, T., and Salminen, A. (2020). Overview of optical digital measuring challenges and technologies in laser welded components in EV battery module design and manufacturing. Batteries *6*, 47. https://doi.org/10.3390/batteries6030047.

153. Biswas, S., Hsieh, A., Juzkow, M., Shan, D.O.U., and Van Tassell, B. (2021). Battery manufacturing

processes based on acoustic and process signal analysis. US Patent.

154. Colthorpe, A. (2025). Recycler Redwood builds 63MWh second-life EV battery microgrid for AI data centre. Energy-Storage.News. https://www.energy-storage.news/recycler-redwood-builds-63mwh-second-life-ev-battery-microgrid-for-ai-data-centre/.

155. Christensen-Jeffries, K., Couture, O., Dayton, P.A., Eldar, Y.C., Hynynen, K., Kiessling, F., O'Reilly, M., Pinton, G.F., Schmitz, G., Tang, M.-X., et al. (2020). Super-resolution ultrasound imaging. Ultrasound Med. Biol. *46*, 865–891. https://doi.org/10.1016/j.ultrasmedbio.2019.11.013.